ABSTRACT

HYBRID EXPLICIT-IMPLICIT FDTD-FEM TIME-DOMAIN SOLVER FOR ELECTROMAGNETIC PROBLEMS

by
Kakhkhor Abdijalilov

The Finite-Difference Time-Domain (FDTD) method and Finite-Element (FEM) method are numerical techniques used for solving Maxwell's electromagnetic equations. FDTD-FEM hybrid methods opt for combining the advantages of both FDTD and FEM. In this dissertation, signal processing techniques were used to analyze the FDTD stability condition. A procedure, which reduces time-sampling error yet preserves the stability of algorithm is proposed. Both explicit and implicit time-stepping schemes were treated in the framework of the developed method. An improved version of the implicit-explicit FEM-FDTD hybrid method was developed. The new method minimizes reflection from the interface between different types of grids. A class of transfer functions with low reflection error for stable hybrid time-stepping was derived. The stability of the method is rigorously proven for a general three-dimensional case.

HYBRID EXPLICIT-IMPLICIT FDTD-FEM TIME-DOMAIN SOLVER FOR ELECTROMAGNETIC PROBLEMS

by
Kakhkhor Abdijalilov

A Dissertation
Submitted to the Faculty of
New Jersey Institute of Technology and
Rutgers, The State University of New Jersey - Newark
in Partial Fulfillment of the Requirements for the Degree of
Doctor of Philosophy in Applied Physics

Federated Physics Department

January 2005

APPROVAL PAGE

HYBRID EXPLICIT-IMPLICIT FDTD-FEM TIME-DOMAIN SOLVER FOR ELECTROMAGNETIC PROBLEMS

Kakhkhor Abdijalilov

Dr. Haim Grebel, Dissertation Advisor — Date
Professor, Department of Electrical and Computer Engineering, NJIT

Dr. John F. Federici, Committee Member — Date
Professor, Department of Applied Physics, NJIT

Dr. Edip Niver, Committee Member — Date
Associate Professor, Department of Electrical and Computer Engineering, NJIT

Dr. Richard V. Snyder, Committee Member — Date
Adjunct Professor, Department of Electrical and Computer Engineering, NJIT
RS Microwave Company Inc., Butler, NJ

Dr. Daniel E. Murnick, Committee Member — Date
Professor, Department of Physics, Rutgers

Dr. Andrei Sirenko, Committee Member — Date
Assistant Professor, Department of Applied Physics, NJIT

BIOGRAPHICAL SKETCH

Author: Kakhkhor Abdijalilov

Degree: Doctor of Philosophy

Date: January 2005

Undergraduate and Graduate Education:

- Doctor of Philosophy in Applied Physics,
  New Jersey Institute of Technology, Newark, NJ, 2005

- Master of Science in Physics,
  Tashkent State University, Tashkent, Uzbekistan, 1997

Major: Applied Physics

Presentations and Publications:

K. Abdijalilov and H. Grebel,
"Z-Transform Theory and FDTD stability,"
IEEE Trans. Antennas Propagat., vol. 52, pp. 2950-2954, Nov. 2004.

K. Abdijalilov and H. Grebel,
"Tunable Explicit-Implicit Hybrid Time-Domain Solver for Electromagnetics,"
submitted to IEEE Trans. Antennas Propagat., Dec. 2004.

To my beloved parents and my wife, Salima

for all their continuous and heartfelt support

ACKNOWLEDGMENT

I would like to express my deepest appreciation and thankfulness to my academic adviser Dr. Haim Grebel not only for valuable and insightful discussions and constant support and encouragement throughout frustrating periods in my research. I would also like to express my gratitude to my Ph. D. dissertation committee members, Dr. John Federici, Dr. Edip Niver, Dr. Richard Snyder, Dr. Daniel Murnick and Dr. Andrei Sirenko for constructive criticism and valuable comments.

TABLE OF CONTENTS

TABLE OF CONTENTS
(Continued)

Chapter **Page**

TABLE OF CONTENTS
(Continued)

Chapter **Page**

LIST OF FIGURES

Figure **Page**

LIST OF FIGURES
(continued)

Figures **Page**

CHAPTER 1

INTRODUCTION

1.1 Computational Electrodynamics

In the study of electromagnetic phenomena, numerical modeling, or, in other words, computer simulations, plays an important role in predicting properties of electronic devices and lowering development cost. Owing to rapid increase in computing capabilities in recent years more complex electromagnetic systems can be accurately modeled even on non-expensive personal computers. In order to effectively utilize available computer resources various numerical methods have been developed.

The goal of computational electrodynamics is to solve Maxwell's equations for electromagnetic fields. For linear medium, Maxwell's equations can be solved either in the time-domain or, the frequency domain. Since, the main subject of this research is time-domain methods, frequency domain methods are briefly commented and only in connection with the main objective. The advantage of using methods in the time-domain is that it can explicitly solve time dependant phenomena such as, broad band pulse propagation: single simulation is enough to solve for a broad range of frequencies.

As its name suggests, Finite-Difference Time-Domain (FDTD) method is a numerical method to solve time-dependant Maxwell's equation using finite-difference approximation of partial derivatives. Since its introduction by Yee [1], FDTD evolved into very effective and arguably the most popular numerical technique for electromagnetic problems [2]. The original FDTD formulation is accurate to the second order both in space and time. Numerical errors are kept small by having a grid spacing

many times smaller than the source wavelength. As shown in Figure 2.1 at the beginning of the Section 2.2, Yee used a three dimensional grid on which electric field nodes are in offset both spatially and temporally from magnetic field nodes. In this way he obtained update equations that express present fields in terms of the past fields throughout the computational domain. The update equations are used to march electric and magnetic fields forward in time. Marching is stopped once the propagation evolves to the desired endpoint. Because of its time-domain nature, FDTD allows to explicitly compute temporal response of the system in addition to frequency response over broad band of frequencies by single simulation.

Despite its simplicity Yee's algorithm did not receive much attention after its publication. One could attribute the lack of interest to the high computational and memory demand of the algorithm and shortcomings of first original formulation such as, its inability to model open problems for long period of time. However, as the cost of computational resources fell and shortcomings of the original FDTD implementation were alleviated, interest in FDTD soared. According to Shlager and Schneider [3], the number of yearly publications from 1985 to 1996 has increased by more than sixty times.

Finite Element method (FEM) [4] is an alternative numerical method for FDTD and is widely used in computational electromagnetic problems. FEM is often used to solve boundary problems in the frequency domain. FEM equations are obtained by applying Galerkin's method (*see chapter 2 for details*): first, the computational domain is divided into small elements of simple form and the solution is expanded in element basis functions. Then, the same basis functions are used as test functions to obtain discrete equations. Since, FEM is formulated in the frequency domain on a nonuniform and

unstructured grid, it does avoid some of the problems inherent to the FDTD such as, time-stepping stability and staircase approximation of curved boundaries. However, accuracy of FEM is dependant on the ability to generate high quality boundary conforming grid. Grid generation is a difficult task by itself; it can significantly increase the computational complexity and hamper implementation of the algorithm.

Current explicit FDTD solvers differ primarily in how the space grid is set up. Most of them use the same second order central difference approximation of the time derivative valid for small time-steps, namely,

$$\frac{\partial f(\xi+\Delta\xi/2)}{\partial\xi} \approx \frac{f(\xi+\Delta\xi)-f(\xi)}{\Delta\xi} \tag{1.1}$$

Marching fields incrementally in time is stable if time-step small enough. Otherwise, exponentially growing discretization error will occur. Stability limit of FDTD is given by the Courant limit [2]

$$\delta t \le \delta t_{\max} \approx \Delta_{\min}/u_{\max} . \tag{1.2}$$

Here Δ_{min} is the smallest cell size in the spatial grid and u_{max} is the maximum wave phase velocity. Because of the bound (1.2), the time-step in many practical applications of FDTD needs to be very small so that errors introduced by approximation (1.1) are negligible. As a result, recent development in FDTD theory has been primarily concerned in reducing spatial discretization errors. At the same, the time-step limit (1.2) has a profound impact on FDTD efficiency: the smaller is the time-step, the more time-steps are needed to complete the simulation. It is clear that, in order to satisfy bound (1.2) for structures with small geometrical features, the time-step need to be much smaller then the accuracy requirement (1.1).

Several approaches have been proposed to overcome the abovementioned problem. Zheng, Chan and Zhang (ZCZ) developed an alternate-direction-implicit (ADI) FDTD algorithm [5] which is free of Courant limit. The time-step used in the algorithm is chosen based on accuracy considerations only. ZCZ algorithm is unconditionally stable and does not require matrix inversion. It uses the same Yee space lattice as the conventional FDTD, and therefore, suffers from the same malady of structured grids: problem arises when trying to employ staircase approximation (*see below*) of curved boundaries.

Another approach to alleviate the restriction imposed by time-step limit (1.2) is to use implicit-explicit hybrid time integration method proposed by Rylander and Bondeson [6,7]. Their scheme employs conventional FDTD with large cell size to discretize homogeneous volumes and FEM with unstructured grid in small volumes around complex boundaries. Stability limit for the hybrid scheme is determined by the cell size for the FDTD section of the domain and is not affected by FEM mesh. Limiting computationally intensive FEM to only small volumes allowed overcoming the Courant limit (1.2) without significantly increasing the math count. One possible drawback of the hybrid method is the artificial reflection from the resulting interface between the two types of grids. The reason for the reflection is the use of different time-stepping methods on each side of the interface.

1.2 Scientific Objective

The main objective of this dissertation was to use discrete-time signal processing techniques [8,9] in order to improve the efficiency of FDTD and FDTD-FEM hybrid

algorithms. Stability of FDTD and the related hybrid algorithm formulation was analyzed using Z-transform and the nonphysical reflection, inherent to any hybrid formulation, was reduced.

CHAPTER 2.

DISCRETIZATION OF MAXWELL'S EQUATIONS

2.1 Governing Equations

Using MKS units, the time-dependant Maxwell's equations are given in differential and integral form by

Faraday's Law:

$$\begin{aligned} \frac{\partial \mathbf{B}}{\partial t} &= -\nabla \times \mathbf{E} - \mathbf{M} \\ \frac{\partial}{\partial t}\iint_A \mathbf{B}\cdot d\mathbf{A} &= -\oint_l \mathbf{E}\cdot d\mathbf{l} - \iint_A \mathbf{M}\cdot d\mathbf{A} \end{aligned} \tag{2.1}$$

Ampere's law

$$\begin{aligned} \frac{\partial \mathbf{D}}{\partial t} &= \nabla \times \mathbf{H} - \mathbf{J} \\ \frac{\partial}{\partial t}\iint_A \mathbf{D}\cdot d\mathbf{A} &= \oint_l \mathbf{H}\cdot d\mathbf{l} - \iint_A \mathbf{J}\cdot d\mathbf{A} \end{aligned} \tag{2.2}$$

In addition to (2.1) and (2.2), electric and magnetic fields must be divergence-less

$$\begin{aligned} \nabla\cdot\mathbf{B} = 0; \qquad & \nabla\cdot\mathbf{D} = 0 \\ \oiint_A \mathbf{B}\cdot d\mathbf{A} = 0; \qquad & \oiint_A \mathbf{D}\cdot d\mathbf{A} = 0 \end{aligned} \tag{2.3}$$

In the above equations, the following (and their MKS units) are defined:

E : electric filed (volts/meter)

D : electric flux density (coulombs/meter^2)

H : magnetic field (amperes/meter)

B : magnetic flux density (webers/meter^2)

A : arbitrary three dimensional surface

dA : differential normal vector that characterizes surface A (meter^2)

l : closed counter that bounds surface A

$d\mathbf{l}$: differential length vector that characterizes contour l (meter)

J : electric current density (amperes/meter^2)

M : equivalent magnetic current density (volts/meter^2)

For linear, isotropic and nondispersive medium materials, the constitutive relations are given by

$$\mathbf{D} = \varepsilon_0 \varepsilon_r \mathbf{E}; \quad \mathbf{B} = \mu_0 \mu \mathbf{H}. \tag{2.4}$$

where free space permittivity $\varepsilon_0 = 8.854 \times 10^{-12}$ farads/meter, free space permeability $\mu_0 = 4\pi \times 10^{-7}$ henrys/meter, and relative permittivity and permeability ε_r, μ_r are dimensionless. For lossy materials, the electric current $\mathbf{J}$ and magnetic current, $\mathbf{M}$, are given by

$$\mathbf{J} = \mathbf{J}_{source} + \sigma \mathbf{E}; \quad \mathbf{M} = \mathbf{M}_{source} + \sigma^* \mathbf{H} \tag{2.5}$$

where σ is electrical conductivity (siemens/meter) and σ^* equivalent magnetic loss (ohms/meter). Magnetic loss term in (2.5) is included mainly for theoretical purposes. Vector components of Maxwell's equations in Cartesian coordinates are given by

$$\frac{\partial H_x}{\partial t} = \frac{1}{\mu}\left[\frac{\partial E_y}{\partial z} - \frac{\partial E_z}{\partial y} - \left(M_{source_x} + \sigma^* H_x\right)\right] \tag{2.6}$$

$$\frac{\partial H_y}{\partial t} = \frac{1}{\mu}\left[\frac{\partial E_z}{\partial x} - \frac{\partial E_x}{\partial z} - \left(M_{source_y} + \sigma^* H_y\right)\right] \tag{2.7}$$

$$\frac{\partial H_z}{\partial t} = \frac{1}{\mu}\left[\frac{\partial E_x}{\partial y} - \frac{\partial E_y}{\partial x} - \left(M_{source_z} + \sigma^* H_z\right)\right] \tag{2.8}$$

$$\frac{\partial E_x}{\partial t} = \frac{1}{\varepsilon}\left[\frac{\partial H_z}{\partial y} - \frac{\partial H_y}{\partial z} - \left(J_{source_x} + \sigma E_x\right)\right] \tag{2.9}$$

$$\frac{\partial E_y}{\partial t} = \frac{1}{\varepsilon}\left[\frac{\partial H_x}{\partial z} - \frac{\partial H_z}{\partial x} - \left(J_{source_y} + \sigma E_y\right)\right] \tag{2.10}$$

$$\frac{\partial E_z}{\partial t} = \frac{1}{\varepsilon}\left[\frac{\partial H_y}{\partial x} - \frac{\partial H_x}{\partial y} - \left(J_{source_z} + \sigma E_z\right)\right] \tag{2.11}$$

The system of above six coupled partial differential equations forms the basis of the FDTD numerical algorithm. The FDTD algorithm need not explicitly enforce Gauss' Law (2.3). This is because these relations are theoretically a direct consequence of the curl equations.

The differential equation for **E** can be obtained by eliminating **H** from (2.2). Using constitutive relations (2.4) and assuming **M** to be zero, one can derive *vector wave equation* for electric the field from (2.1) and (2.2)

$$\nabla \times \mu^{-1} \nabla \times \mathbf{E} + \varepsilon \partial_t^2 \mathbf{E} = -\partial_t \mathbf{J}. \tag{2.12}$$

Similarly, one can eliminate **E** to derive an equation for **H** to get

$$\nabla \times \varepsilon^{-1} \nabla \times \mathbf{H} + \mu \partial_t^2 \mathbf{H} = \nabla \times \left(\frac{1}{\varepsilon}\mathbf{J}\right). \tag{2.13}$$

Solutions of the vector wave equations (2.12) and (2.13) also satisfy Gauss' Law. These equations are the basis of FEM numerical algorithm. The right hand side of (2.13) contains a curl of the total current **J**. When the medium is lossy one relates the current density **J** to the electric field **E** through Ohm's Law (2.5). Tangential component of electric field does vanish on perfectly conducting surfaces, which will allow to decrease the number of unknown discrete field values and result in lower memory storage and operational count of the algorithm (*see Section* 2.3). Because of these reasons, numerical

approach of equation (2.12) for the electric field is preferable over equation (2.13) for the magnetic field.

2.2. Yee's Algorithm

Original Yee's FDTD algorithm for lossless isotropic medium [1] uses rectangular grid with magnetic and electric fields staggered both in time and space as shown in Figure 2.1. The algorithm solves for both electric and magnetic fields in time and space using the coupled Maxwell's curl equations. In order to simplify the derivation of discrete equations let us introduce convenient notation for space points and functions of space and time. Let us denote a space point in a uniform, rectangular lattice as,

$$(i, j, k) = (i\Delta x, j\Delta y, k\Delta z). \tag{2.14}$$

Here, Δx, Δy, Δz are, respectively, the lattice space increments in the x, y, and z coordinate directions, and i, j, and k are either integer or semi integer. Further, let us denote any function evaluated at discrete point in the grid and a discrete point in time as,

$$u(i\Delta x, j\Delta y, k\Delta z, n\Delta t) = u^n_{i,j,k} \tag{2.15}$$

where, Δt is the time increment, n is either integer or, semi-integer.

Let us start with (2.9): the x-component of (2.2) may be written as,

$$\frac{\partial E_x}{\partial t} = \frac{1}{\varepsilon}\left[\frac{\partial H_z}{\partial y} - \frac{\partial H_y}{\partial z} - \left(J_{source_x} + \sigma E_x\right)\right] \tag{2.16}$$

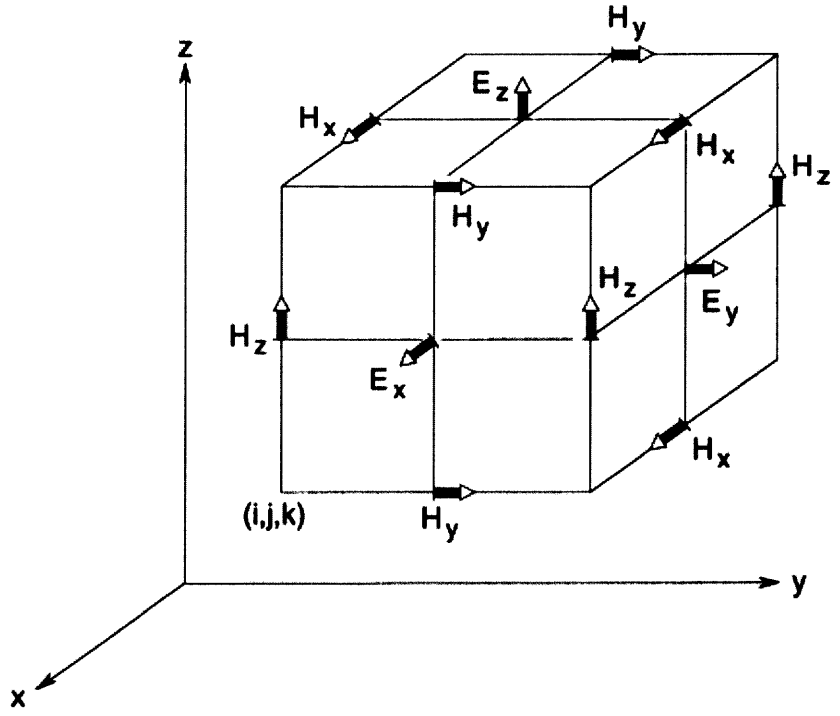

Figure 2.1 Position of the electric (E) and magnetic field (H) vector components about a unit of Yee's space lattice
Source: Taflove, Hagness [2]

Referring to Figure 2.1, substitution of central difference approximation (1.1) for time and space derivatives gives us

$$\varepsilon_{i,j+1/2,k+1/2} \cdot \frac{E_x\Big|_{i,j+1/2,k+1/2}^{n+1/2} - E_x\Big|_{i,j+1/2,k+1/2}^{n-1/2}}{\Delta t} = \frac{H_z\Big|_{i,j+1,k+1/2}^{n} - H_z\Big|_{i,j,k+1/2}^{n}}{\Delta y} - \frac{H_y\Big|_{i,j+1/2,k+1}^{n} - H_y\Big|_{i,j+1/2,k}^{n}}{\Delta z} - J_{source_x}\Big|_{i,j+1/2,k+1/2}^{n} - \sigma_{i,j+1/2,k+1/2} E_x\Big|_{i,j+1/2,k+1/2}^{n}. \tag{2.17}$$

The assumption is that values of E_x at time step n are not stored in the computer memory. Therefore one may use second-order accurate interpolation to approximate the electric field on the right hand side of (2.17) as,

$$E_x\Big|_{i,j+1/2,k+1/2}^{n} = \frac{E_x\Big|_{i,j+1/2,k+1/2}^{n+1/2} + E_x\Big|_{i,j+1/2,k+1/2}^{n-1/2}}{2}. \tag{2.18}$$

Substituting (2.18) into (2.17) leads to

$$E_x\Big|_{i,j+1/2,k+1/2}^{n+1/2} = \left(\frac{1-\dfrac{\Delta t\sigma_{i,j+1/2,k+1/2}}{2\varepsilon_{i,j+1/2,k+1/2}}}{1+\dfrac{\Delta t\sigma_{i,j+1/2,k+1/2}}{2\varepsilon_{i,j+1/2,k+1/2}}}\right) E_x\Big|_{i,j+1/2,k+1/2}^{n-1/2}$$
$$+\left(\frac{\dfrac{\Delta t}{2\varepsilon_{i,j+1/2,k+1/2}}}{1+\dfrac{\Delta t\sigma_{i,j+1/2,k+1/2}}{2\varepsilon_{i,j+1/2,k+1/2}}}\right)\cdot\left(\frac{H_z\Big|_{i,j+1,k+1/2}^{n}-H_z\Big|_{i,j,k+1/2}^{n}}{\Delta y}-\frac{H_y\Big|_{i,j+1/2,k+1}^{n}-H_y\Big|_{i,j+1/2,k}^{n}}{\Delta z}-J_{source_x}\Big|_{i,j+1/2,k+1/2}^{n}\right). \tag{2.19}$$

Discretization of the x-component in (2.1) similarly gives us

$$H_x\Big|_{i-1/2,j+1,k}^{n+1} = \left(\frac{1-\dfrac{\Delta t\sigma^*_{i-1/2,j+1,k}}{2\mu_{i-1/2,j+1,k}}}{1+\dfrac{\Delta t\sigma^*_{i-1/2,j+1,k}}{2\mu_{i-1/2,j+1,k}}}\right) H_x\Big|_{i-1/2,j+1,k}^{n}$$
$$+\left(\frac{1-\dfrac{\Delta t}{2\mu_{i-1/2,j+1,k}}}{1+\dfrac{\Delta t\sigma^*_{i-1/2,j+1,k}}{2\mu_{i-1/2,j+1,k}}}\right)\cdot\left(\frac{E_y\Big|_{i-1/2,j+1,k+1/2}^{n+1/2}-E_y\Big|_{i-1/2,j+1,k-1/2}^{n+1/2}}{\Delta z}-\frac{E_z\Big|_{i-1/2,j+3/2,k}^{n+1/2}-E_z\Big|_{i-1/2,j+1/2,k}^{n+1/2}}{\Delta y}-M_{source_x}\Big|_{i-1/2,j+1,k}^{n+1/2}\right). \tag{2.20}$$

The equations for the other components of electric and magnetic fields are given by,

$$E_y\Big|_{i-1/2,j+1,k+1/2}^{n+1/2} = \left(\frac{1-\dfrac{\Delta t\sigma_{i-1/2,j+1,k+1/2}}{2\varepsilon_{i-1/2,j+1,k+1/2}}}{1+\dfrac{\Delta t\sigma_{i-1/2,j+1,k+1/2}}{2\varepsilon_{i-1/2,j+1,k+1/2}}}\right) E_{i-1/2,j+1,k+1/2}^{n-1/2}$$
$$+\left(\frac{\dfrac{\Delta t}{\varepsilon_{i-1/2,j+1,k+1/2}}}{1+\dfrac{\Delta t\sigma_{i-1/2,j+1,k+1/2}}{2\varepsilon_{i-1/2,j+1,k+1/2}}}\right)\cdot\left(\frac{H_x\Big|_{i-1/2,j+1,k+1}^{n}-H_x\Big|_{i-1/2,j+1,k}^{n}}{\Delta z}-\frac{H_z\Big|_{i,j+1,k+1/2}^{n}-H_z\Big|_{i-1,j+1,k+1/2}^{n}}{\Delta x}-J_{source_y}\Big|_{i-1/2,j+1,k+1/2}^{n}\right) \quad (2.21)$$

$$H_y\Big|_{i,j+1/2,k+1}^{n+1} = \left(\frac{1-\dfrac{\Delta t\sigma^*_{i,j+1/2,k+1}}{2\mu_{i,j+1/2,k+1}}}{1+\dfrac{\Delta t\sigma^*_{i,j+1/2,k+1}}{2\mu_{i,j+1/2,k+1}}}\right) H_y\Big|_{i,j+1/2,k+1}^{n}$$
$$+\left(\frac{\dfrac{\Delta t}{\mu_{i,j+1/2,k+1}}}{1+\dfrac{\Delta t\sigma^*_{i,j+1/2,k+1}}{2\mu_{i,j+1/2,k+1}}}\right)\cdot\left(\frac{E_z\Big|_{i+1/2,j+1/2,k+1}^{n+1/2}-E_z\Big|_{i+1/2,j+1/2,k+1}^{n+1/2}}{\Delta x}-\frac{E_x\Big|_{i,j+1/2,k+3/2}^{n+1/2}-E_x\Big|_{i,j+1/2,k+1/2}^{n+1/2}}{\Delta z}-M_{source_y}\Big|_{i,j+1/2,k+1}^{n+1/2}\right) \quad (2.22)$$

$$E_z\Big|_{i-1/2,j+1/2,k+1}^{n+1/2} = \left(\frac{1-\dfrac{\Delta t\sigma_{i-1/2,j+1/2,k+1}}{2\varepsilon_{i-1/2,j+1/2,k+1}}}{1+\dfrac{\Delta t\sigma_{i-1/2,j+1/2,k+1}}{2\varepsilon_{i-1/2,j+1/2,k+1}}}\right) E_{i-1/2,j+1/2,k+1}^{n-1/2}$$
$$+\left(\frac{\dfrac{\Delta t}{\varepsilon_{i-1/2,j+1/2,k+1}}}{1+\dfrac{\Delta t\sigma_{i-1/2,j+1/2,k+1}}{2\varepsilon_{i-1/2,j+1/2,k+1}}}\right)\cdot\left(\frac{H_y\Big|_{i,j+1/2,k+1}^{n}-H_y\Big|_{i-1,j+1/2,k+1}^{n}}{\Delta x}-\frac{H_x\Big|_{i-1/2,j+1,k+1}^{n}-H_x\Big|_{i-1/2,j+1,k+1}^{n}}{\Delta y}-J_{source_z}\Big|_{i-1/2,j+1/2,k+1}^{n}\right) \quad (2.23)$$

$$H_z\Big|_{i,j+1,k+1/2}^{n+1} = \left(\frac{1-\dfrac{\Delta t\sigma^*_{i,j+1,k+1/2}}{2\mu_{i,j+1,k+1/2}}}{1+\dfrac{\Delta t\sigma^*_{i,j+1,k+1/2}}{2\mu_{i,j+1,k+1/2}}}\right) H_y\Big|_{i,j+1,k+1/2}^{n}$$
$$+\left(\frac{\dfrac{\Delta t}{\mu_{i,j+1,k+1/2}}}{1+\dfrac{\Delta t\sigma^*_{i,j+1,k+1/2}}{2\mu^*_{i,j+1,k+1/2}}}\right)\cdot\left(\frac{E_x\Big|_{i,j+3/2,k+1/2}^{n+1/2} - E_x\Big|_{i,j+1/2,k+1/2}^{n+1/2}}{\Delta y} - \frac{E_y\Big|_{i+1/2,j+1,k+1/2}^{n+1/2} - E_y\Big|_{i-1/2,j+1,k+1/2}^{n+1/2}}{\Delta x} - M_{source_z}\Big|_{i,j+1,k+1/2}^{n+1/2}\right) \tag{2.24}$$

A full set of FDTD equations can be written in symbolic matrix form as,

$$\mathbf{E}^{n+1/2} = \mathbf{A}_E\mathbf{E}^{n-1/2} + \mathbf{B}_E\mathbf{H}^n + \mathbf{C}_E\mathbf{J}^n_{source} \tag{2.25}$$

for the electric field and as,

$$\mathbf{H}^{n+1} = \mathbf{A}_H\mathbf{H}^n + \mathbf{B}_H\mathbf{E}^{n+1/2} + \mathbf{C}_H\mathbf{M}^{n+1/2}_{source} \tag{2.26}$$

for the magnetic field.

If the electric field at time-step n-1/2 and the magnetic field at time-step n are known throughout the grid, electric fields at the next time-step n can be found from (2.25), which in turn will allow to update the magnetic fields to the next time-step n+1 by using (2.26). This process which is called *leapfrogging*, allows to march fields forward to any desired future time.

FDTD equations (2.19)-(2.24) are derived from the system of coupled equations (2.1) and (2.2). Another approach is to apply central difference approximation of derivatives to the vector wave equation instead of applying it to Maxwell's coupled equations. The resulting finite-difference scheme is equivalent to the Yee's algorithm [10] and also referred to as FDTD. For source free region spatial discretization of two dimensional transverse electric mode (TEM) $E_z = 0$ leads to

$$\varepsilon\mu\frac{\partial^2}{\partial t^2}E_x\Big|_{i,j+1/2}=\frac{E_x\Big|_{i,j+3/2}-2E_x\Big|_{i,j+1/2}+E_x\Big|_{i,j-1/2}}{\Delta y^2}-\frac{E_y\Big|_{i+1/2,j+1}+E_y\Big|_{i-1/2,j}-E_y\Big|_{i-1/2,j+1}-E_y\Big|_{i+1/2,j}}{\Delta x\Delta y} \tag{2.27}$$

$$\varepsilon\mu\frac{\partial^2}{\partial t^2}E_y\Big|_{i+1/2,j}=\frac{E_y\Big|_{i+3/2,j}-2E_y\Big|_{i+1/2,j}+E_y\Big|_{i-1/2,j}}{\Delta x^2}-\frac{E_x\Big|_{i+1,j+1/2}+E_x\Big|_{i,j-1/2}-E_x\Big|_{i,j+1/2}-E_x\Big|_{i+1,j}}{\Delta x\Delta y} \tag{2.28}$$

Time discretization of these equations is discussed in the next section. It is shown that FDTD for vector wave equation is equivalent to FEM with rectangular elements with trapezoidal integration of stiffness and mass matrices.

2.3 Finite Element Method

Finite Element method [4] is an alternative numerical technique to FDTD and is also used to solve Maxwell's equations. In order to discretize fields in space, the simulation domain is divided into small segments of simple forms. The resulting mesh can be unstructured and nonuniform. Unstructured mesh is a mesh whose segments (elements) are not naturally indexed (*i,j,k*) as a multidimensional array. Triangular elements are often used for 2D problems, whereas 3D problems are often solved using tetrahedral elements. Other element types are also possible [4]. Two or three dimensional rectangular elements result in uniform grid equivalent to FDTD spatial discretization. Example of two dimensional triangular grid is shown in Figure 2.4 in Section 2.5. Basis functions are associated with each element. These functions are chosen to accurately represent solutions within each element. If elements are small enough, only a few basis functions are need. Basis

functions are assumed to be nonzero only within their element. Vector functions, also refereed to as edge elements, described by Whitney [11] and discussed by Nedelec [12] are most suitable as basis functions for 2D and 3D electromagnetic problems [4]. Edge elements are divergence free and preserve tangential continuity of the fields. Below, a short review of FEM method is presented.

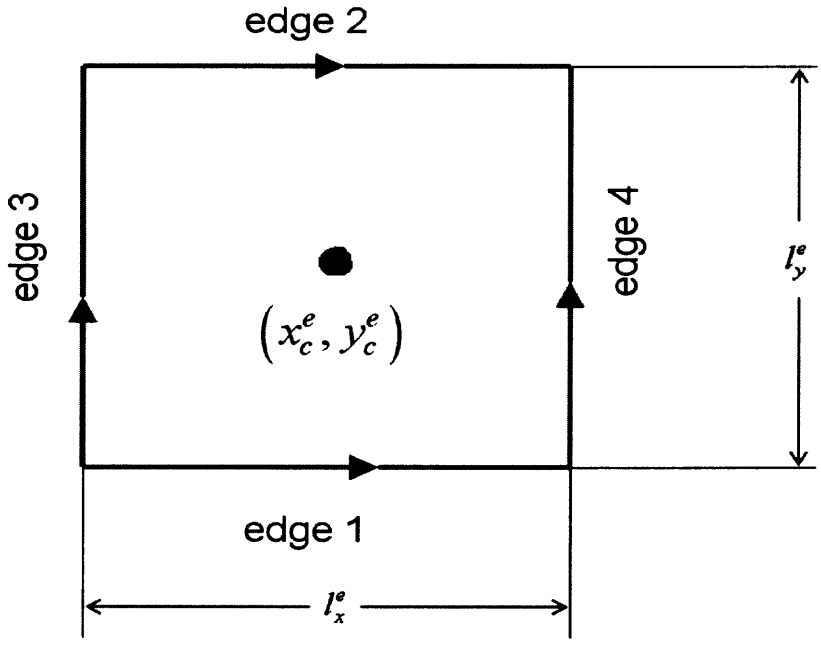

Figure 2.2 Rectangular edge element

Two dimensional rectangular and triangular edge elements are shown in Figure 2.2 and Figure 2.3 respectively. Let us consider the rectangular element first. Associated with each edge of the rectangle is a vector basis function. Four basis functions are defined:

$$\mathbf{N}_1^e = \frac{1}{l_y^e}\left(y_c^e + \frac{l_y^e}{2} - y\right)\hat{x} \tag{2.29}$$

$$\mathbf{N}_2^e = \frac{1}{l_y^e}\left(y - y_c^e + \frac{l_y^e}{2}\right)\hat{x} \tag{2.30}$$

$$\mathbf{N}_3^e = \frac{1}{l_x^e}\left(x_c^e + \frac{l_c^e}{2} - x\right)\hat{y} \tag{2.31}$$

$$\mathbf{N}_3^e = \frac{1}{l_x^e}\left(x - x_c^e + \frac{l_c^e}{2}\right)\hat{y} \tag{2.32}$$

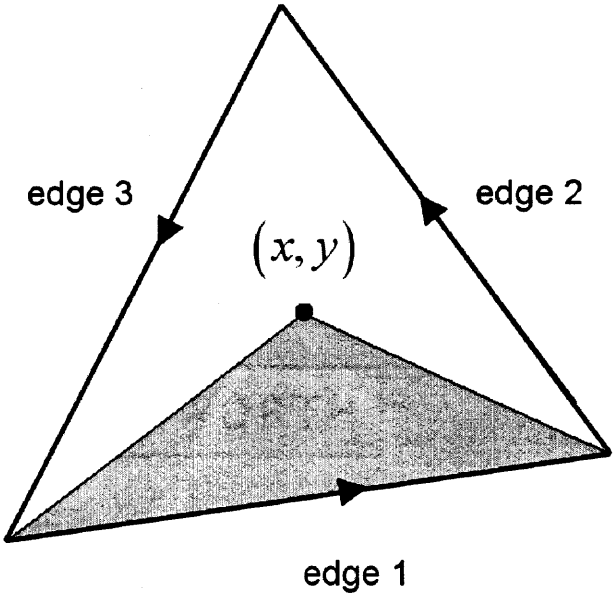

Figure 2.3 Triangular edge element

An important feature of these basis functions is that $\mathbf{N}_i^e$ has a tangential component only along the *i*th edge and not along the other edges. Thus, the continuity of the tangential field across all element edges is guaranteed. Another unique feature of these functions is that each satisfies the divergence conditions $\nabla \cdot \mathbf{N}_i^e = 0$ within the element. Therefore, they are ideal for representing source-free regions. The major disadvantage of using rectangular elements is that they are restricted to a limited class of geometries. When one deals with problems having irregular geometries, triangular elements are more suitable

for spatial discretization. In the next section advantages and disadvantages of triangular and rectangular grids are discussed in more details.

Similar to the rectangular case, vector basis functions for triangular elements are divergence-free and guarantee the tangential continuity of the numerical solution. Three basis functions are associated with each edge and are defined as [4],

$$\mathbf{N}_1^e = \left(L_1^e \nabla L_2^e - L_2^e \nabla L_1^e\right) l_1^e \tag{2.33}$$

$$\mathbf{N}_2^e = \left(L_2^e \nabla L_3^e - L_3^e \nabla L_2^e\right) l_2^e \tag{2.34}$$

$$\mathbf{N}_3^e = \left(L_3^e \nabla L_1^e - L_1^e \nabla L_3^e\right) l_3^e \tag{2.35}$$

where, l_i^e is the length of ith element and L_i^e is are of the triangle formed by the ith edge and observation point (x, y) inside the element. For example, area of the shaded triangle in Figure 2.3 equals to L_1^e.

Once the basis functions are defined, an approximate solution within the element can be expressed using local indices as,

$$\mathbf{E}^e = \sum_i \mathbf{N}_i^e E_i^e , \tag{2.36}$$

where, E_i^e, denotes the tangential field along the ith edge and summation is carried out over all elements' edges.

Let us consider Maxwell's curl-curl equations for the electric field,

$$\nabla \times \mu^{-1} \nabla \times \mathbf{E} + \varepsilon \partial_t^2 \mathbf{E} = -\partial_t \mathbf{J}_{source} . \tag{2.37}$$

The first step in deriving FEM equations is to assume that a numerical solution can be expanded in terms of the element basis functions as,

$$\mathbf{E} = \sum_e \mathbf{E}^e = \sum_e \sum_i \mathbf{N}_i^e (\mathbf{r}) E_i^e (t) . \tag{2.38}$$

It should be noted that the basis functions, $\mathbf{N}_i^e(\mathbf{r})$, in (2.38) are time-independent, whereas unknowns or degrees of freedom associated with edges, $E_i^e(t)$, do depend on time only. In order to derive FEM equations, the Galerkin's method is applied to the governing equation: expansion of **E** in terms of its basis function (2.38) is substituted into (2.37), then, the equation is multiplied by every basis function and integrated over the respective element volume. The resulting system of equations can be written as,

$$\mathbf{S}\mathbf{u}(t) + \mathbf{M}\partial_t^2\mathbf{u}(t) = -\mathbf{f}(t) \tag{2.39}$$

where the stiffness matrix **S**, mass matrix **M** and source term, **f**(t), are assembled from elements' matrices by using conversion from local to global indices [4]. The unknown vector of solution, **u**(t), represents the electric field, $E_i^e(t)$, in terms of the global indices. The stiffness and mass matrices for each element are given by [4]

$$\begin{aligned} S_{ij}^e &= \int \mu^{-1}\nabla\times\mathbf{N}_i^e\cdot\nabla\times\mathbf{N}_j^e dv \\ M_{ij}^e &= \int \varepsilon\mathbf{N}_i^e\cdot\mathbf{N}_j^e dv \\ f_i^e &= \int \mathbf{N}_i^e\cdot\partial_t\mathbf{J}_{source} dv \end{aligned} \tag{2.40}$$

The matrix equation (2.39) can be solved either in the frequency domain or, in time-domain. Since, the objective of this thesis is to investigate hybrid schemes, only time-domain solutions of (2.39) are discussed below.

2.4 Time-Domain Discretization

There are many ways to time-discretize equation (2.39) [4]. Some of them are discussed in this section.

A central difference method is second-order accurate:

$$\partial_t^2 \mathbf{u}^n \approx \frac{\mathbf{u}^{n+1} - 2\mathbf{u}^n + \mathbf{u}^{n-1}}{\Delta t^2}. \tag{2.41}$$

Substituting (2.41) into (2.39) leads to an update equation

$$\frac{1}{\Delta t^2}\mathbf{M}\mathbf{u}^{n+1} = -\mathbf{f}^n - \mathbf{S}\mathbf{u}^n + \frac{1}{\Delta t^2}\mathbf{M}\left(2\mathbf{u}^n - \mathbf{u}^{n-1}\right) \tag{2.42}$$

Apart from inverting the mass matrix **M** (*which can be diagonal* [4]), equation (2.42) explicitly expresses the vector of unknowns, $\mathbf{u}^{n+1}$, in terms of previous field values. Therefore, time-discretization (2.41) is said to be *explicit*. The resulting time-marching is stable provided that the time step, Δt, is sufficiently small. Elemental stiffness and mass matrices defined by (2.40) can be evaluated numerically. It is straightforward to verify that trapezoidal integration with rectangular basis functions as defined in (2.29)-(2.32) makes the mass matrix **M** in (2.39) diagonal. The resulting time-domain FEM is equivalent to central difference time-discretization of vector wave finite-difference equations (2.27) and (2.28) [10].

On the other, a backward difference approximation

$$\partial_t^2 \mathbf{u}^n \approx \frac{\mathbf{u}^n - 2\mathbf{u}^{n-1} + \mathbf{u}^{n-2}}{\Delta t^2} \tag{2.43}$$

is only first-order accurate yet results in an unconditionally stable scheme, i.e. time-marching is stable regardless of the choice of Δt [4]. The resulting time-stepping is *implicit* and given by,

$$\left(\frac{1}{\Delta t^2}\mathbf{M} + \mathbf{S}\right)\mathbf{u}^n = -\mathbf{f}^n + \frac{1}{\Delta t^2}\mathbf{M}\left(2\mathbf{u}^{n-1} - \mathbf{u}^{n-2}\right) \tag{2.44}$$

The system of matrices (2.44) is not diagonal and needs to be inverted in order to march fields forward in time.

Many other schemes are described by Ghrist et al [13]. Application of discrete-time signal processing techniques to construct new time-stepping schemes is investigated by Abdijalililov and Grebel [36]. A detailed discussion of the approach is presented below in Chapter 5.

2.5 FDTD and FEM Comparison

In this section, FDTD and time-domain FEM are compared and the advantages and disadvantages of both methods are discussed.

As mentioned above, the main advantage of FDTD is its simplicity and ease of implementation. FDTD update equations are explicit, suitable for parallel processing out of the box. Indeed, as it can be seen from equations (2.19)-(2.24), all nodes are updated independently of each other and, for homogeneous volumes, the update equations are identical. Rectangular grid of FDTD is straightforward to generate and well-suited for solving structures with large homogeneous volumes. At the same time, rectangular grids do not conform well to curved boundaries. A staircase approximation of curved boundaries, shown in Figure 2.5, results in high discretization error. A small cell size is required in order to reduce the error: this, in turn, increases both the operational count and memory storage requirements for the algorithm. Explicit time-stepping is subject to the stability bound (1.2). Small cell size also forces the time-step to be small. Decreasing the time-step size increases the number of time-steps needed to evolve propagating electromagnetic fields to the desired endpoint. Therefore, the operational count of the algorithm increases because of an increased number of cells and an increased number of time-steps. These considerations make FDTD in its original form an inefficient approach

for modeling structures with geometrical features much smaller than the wavelength of the source.

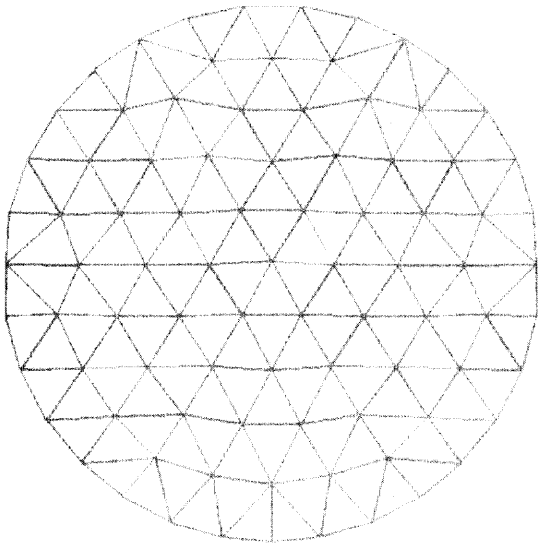

Figure 2.4 Example of two dimensional unstructured triangular grid

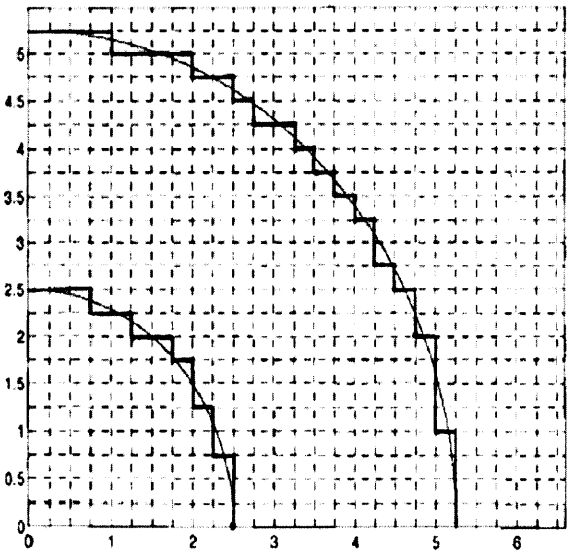

Figure 2.5 FDTD staircase approximation

FEM with an unstructured grid is well suited for modeling structures with curved boundaries. It can be seen from Figure 2.4 that triangular mesh conforms to the circular boundary very well, despite the fact that the average triangle size is larger than the cell size of rectangular cell shown in Figure 2.5. Therefore, spatial discretization error of FEM approximation can be made small without significantly increasing the number of elements . In general, the mass matrix, **M,** in the update equation (2.42) is not diagonal. Hence, matrix inversion may be required to solve the FEM equations even if explicit time-discretization scheme is used. Also, the stability bound on the time-step for triangular elements is lower. And last, but not least, the accuracy of FEM solution

depends on the grid quality. Grid generation is a difficult task by itself. Spatial discretization error may be high if some of the triangles have small angles or, the triangle edges do not fit well to the curved boundaries [14].

As a conclusion, it can be said that FDTD and FEM are complementary techniques to deal with different types of problems. This may suggest that a hybrid FEM-FDTD approach would take advantages of both methods. Various hybrids methods have been developed. Chapter 6 discusses hybridization of time-stepping strategy in more details.

2.6 Generalized FDTD Algorithm

As was discussed in the previous section, an orthogonal grid of Yee's FDTD approach does not permit accurate modeling of curved boundaries. Additional error results in the event that vertexes of rectangular elements do not conform to the shape of a physical boundary, . Due to this error, FDTD solution may not converge to the correct answer in the presence of *perfect conductor* (PC) boundaries, no matter how fine the mesh is made [15]. As a result, FDTD algorithms using boundary-fitted grids have been developed [16,17,18].

Modified FDTD is constructed by applying Ampere's law and Faraday's law in integral form to the generalized Yee's lattice. Example of generalized unstructured lattice with hexahedral cell is shown in Figure 2.7. The resulting update equations are fully explicit and similarly to conventional formulation, can be written in matrix form, (2.25) and (2.26). Detailed derivation of time-marching equations is considered by Gedney and Lansing [18]. The stability of the algorithm is discussed in Chapter 5.

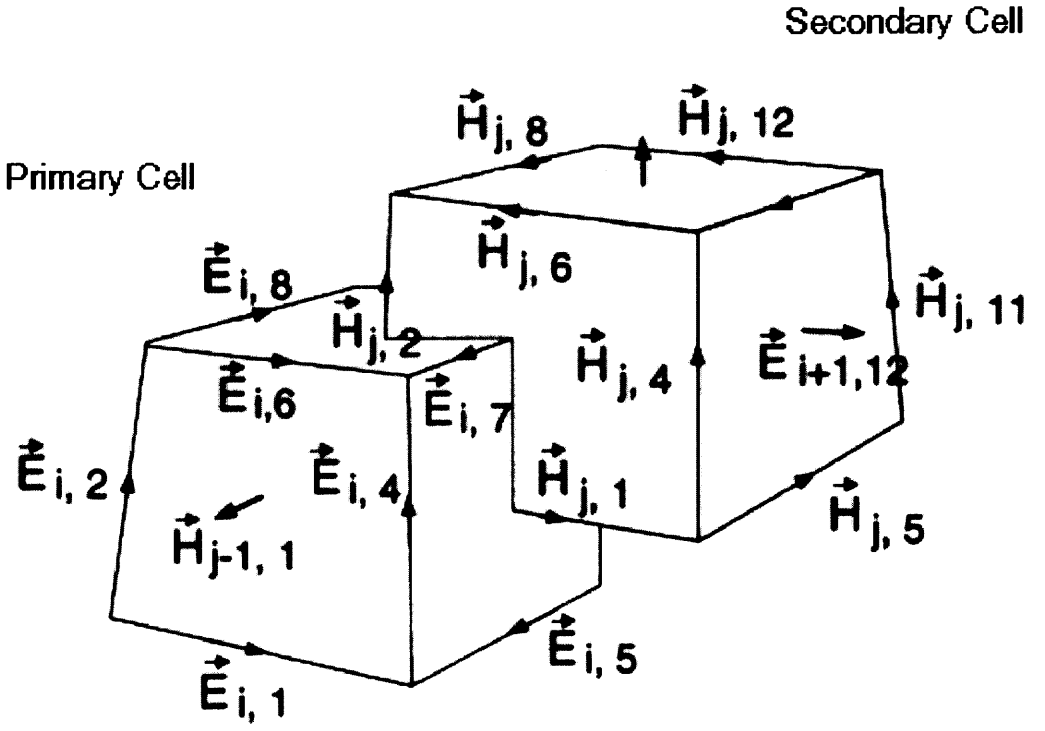

Figure 2.b A generalized unstructured Yee lattice using hexahedral cells.
Source: Taflove, Hagness [2]

CHAPTER 3

FDTD NUMERICAL DISPERSION AND STABILITY

3.1 Derivation of Numerical Dispersion Relation

The FDTD algorithm for Maxwell's equations reviewed in Chapter 2 results in nonphysical dispersion of simulated waves even in the case of a free-space computational lattice. That is, phase velocity of the numerical wave modes depends on wavelength and direction of propagation. Numerical dispersion results in an accumulated phase error for the propagating waves that can lead to nonphysical results such as, broadening and ringing of a pulsed waveform, imprecise cancellation of multiple scattered waves, anisotropy, and pseudorefraction. Numerical dispersion is a factor in FDTD modeling that must be accounted for in order to understand its accuracy limits, especially for electrically large problems.

FDTD numerical dispersion is the relation between frequency and numerical wave vector in free space. Dispersion relation is derived by substituting the vector-field traveling-wave expression,

$$\begin{aligned} \mathbf{E}^n_{I,J,K} &= \mathbf{E}_0 e^{j\left(\omega n\Delta t - \tilde{k}_x I\Delta x - \tilde{k}_y J\Delta y - \tilde{k}_z K\Delta z\right)} \\ \mathbf{H}^n_{I,J,K} &= \mathbf{H}_0 e^{j\left(\omega n\Delta t - \tilde{k}_x I\Delta x - \tilde{k}_y J\Delta y - \tilde{k}_z K\Delta z\right)} \end{aligned}, \tag{3.1}$$

into FDTD time-stepping equations (2.19)-(2.24) and with, $\varepsilon = \varepsilon_0$, $\mu = \mu_0$, $\sigma = \sigma^* = 0$. Manipulation of the equations can be significantly simplified if compact vector notations introduced by Taflove and Brodwin are used [19]. Numerical dispersion of Yee's algorithm in three dimensions is given by [2],

$$\left[\frac{1}{c\Delta t}\sin\left(\frac{\Omega\Delta t}{2}\right)\right]^2=\left[\frac{1}{\Delta x}\sin\left(\frac{\tilde{k}_x\Delta x}{2}\right)\right]^2+\left[\frac{1}{\Delta y}\sin\left(\frac{\tilde{k}_y\Delta y}{2}\right)\right]^2 +\left[\frac{1}{\Delta z}\sin\left(\frac{\tilde{k}_z\Delta z}{2}\right)\right]^2. \tag{3.2}$$

Two-dimensional and one-dimensional dispersion relations are obtained from (3.2) by letting the corresponding wave vector components to be zero, $k_y = 0$, $k_z = 0$. It is seen from (3.2) that the FDTD dispersion relation is nonlinear and anisotropic, which leads to important consequences discussed below.

3.2 Comparison with Ideal Dispersion Relation

In contrast to the numerical dispersion relation (3.2), the analytical dispersion relation for physical plane wave propagating in three dimensional free space is simply,

$$\frac{\Omega^2}{c^2}=k_x^2+k_y^2+k_z^2. \tag{3.3}$$

In general, numerical dispersion relation and physical dispersion relation result in different wave vectors for the propagating plane wave, namely $\mathbf{k}\neq\tilde{\mathbf{k}}$. However, as the grid cell size, Δx, Δy, Δz, and time step, Δt, approach zero, the two dispersion relations become identical. Two-dimensional, dispersion error for different cell-size–to-wavelength ratio, N_λ, and propagation angles, $0\le\phi\le 90^0$, is shown in Figure 3.1. The *Courant stability factor*, $S=c\Delta t/\Delta$, is defined with $\Delta=\Delta x=\Delta y$. It can be seen that the numerical phase velocity, v_p, is smaller than the speed of light, c, and is a function of both propagation angle and cell size-to-wavelength ratio. It is also clear that errors due to inaccurate numerical velocities are cumulative, i.e. they increase linearly with the wave-

propagation distance. These errors represent a fundamental limitation of all grid based solvers, and play an important role when modeling electrically large structures.

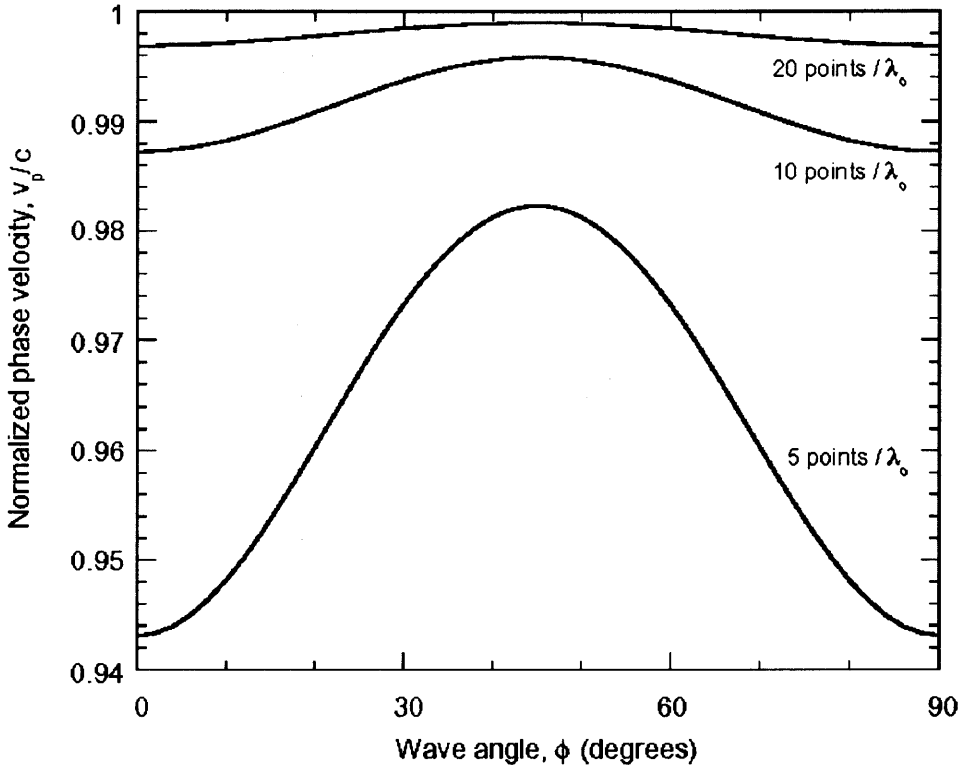

Figure 3.1 Variation of two dimensional numerical phase velocity with wave-propagation angle. $S = c\Delta t/\Delta = 0.5$ for all three cases
Source: Taflove, Hagness [2]

3.3 Numerical Stability

Time-marching of FDTD need to be stable, i.e. the linear system of (2.25) and (2.26) should not have solutions which exponentially grow as function of time-step, $\sim \alpha^n$, $|\alpha| > 1$. Otherwise, the numerical error, though initially small, will grow and eventually overcome the solution [20]. Stable regime of FDTD operation can be established from the dispersion relation (3.2) by employing complex-frequency analysis [2]. Exponentially growing solutions would have complex-valued, normalized angular

frequency, $\omega = \Omega\Delta t$. If the imaginary part of ω is negative, numerical plane wave growths factor, α, can be estimated as

$$\left|e^{j\omega n}\right| = e^{-n\,\mathrm{Im}(\omega)} = \alpha^n, \quad \alpha = e^{-\mathrm{Im}(\omega)} > 1 \tag{3.4}$$

Therefore, FDTD is stable if the angular frequency in (3.2) is real valued for all possible real-valued numerical wave vector components. For convenience, let us rewrite dispersion relation as,

$$\begin{aligned}\left[\sin\left(\frac{\Omega\Delta t}{2}\right)\right]^2 = (c\Delta t)^2\left[\frac{1}{\Delta x}\sin\left(\frac{\tilde{k}_x\Delta x}{2}\right)\right]^2 + (c\Delta t)^2\left[\frac{1}{\Delta y}\sin\left(\frac{\tilde{k}_y\Delta y}{2}\right)\right]^2 \\ + (c\Delta t)^2\left[\frac{1}{\Delta z}\sin\left(\frac{\tilde{k}_z\Delta z}{2}\right)\right]^2.\end{aligned} \tag{3.5}$$

Since, the angular frequency is allowed to be real-valued only, the right hand side of (3.5) must be bounded by 1 for any wave vector. Estimating the maximum value for the right hand side of (3.5) provides us with the stability limit of FDTD time-marching as,

$$\Delta t \le \frac{1}{c\sqrt{(\Delta x)^{-2} + (\Delta y)^{-2} + (\Delta z)^{-2}}} \equiv \Delta t_{3D} \tag{3.6}$$

Stability limit (3.6) is derived for 3D case. Two dimensional and one dimensional equivalents of it are obtained simply by omitting Δz or, Δy to get,

$$\begin{aligned}\Delta t &\le \frac{1}{c\sqrt{(\Delta x)^{-2} + (\Delta y)^{-2}}} \equiv \Delta t_{2D} \\ \Delta t &\le \frac{\Delta x}{c} \equiv \Delta t_{1D}.\end{aligned} \tag{3.7}$$

For the grid with equilateral cell, $\Delta x = \Delta y = \Delta z$, (3.6) and (3.7) can be simplified as,

$$t_{ND} = \frac{\Delta x}{c\sqrt{N}}; \quad N = 1, 2, 3 \tag{3.8}$$

where, N is the dimensionality of the domain.

As was mentioned above, stability-limit on the time-step size is an important limiting factor for FDTD efficiency. Due to the bound (3.6), many practical applications require smaller time-step than it would be needed in order to resolve the fastest spectral component of the electromagnetic wave. With a smaller time-step, more iterations and therefore, more computational time, are needed. Several approaches to overcome the time-step limit of conventional FDTD have been proposed and are detailed in Chapter 6.

CHAPTER 4

Z-TRANSFORM THEORY

4.1 Discrete-Time Systems

A discrete-time system is defined as a transformation of input sequence, $x[n]$, into an output sequence, $y[n]$ such that,

$$y[n] = \hat{T}\{x[n]\}. \tag{4.1}$$

Among all possible discrete-time transformations, the linear time-invariant (LTI) systems deserve special attention. The class of linear systems is defined by the principle of superposition,

$$\hat{T}\{a_1 x_1[n] + a_2 x_2[n]\} = a_1 \hat{T}\{x_1[n]\} + a_2 \hat{T}\{x_2[n]\} \tag{4.2}$$

A time-invariant system is a system for which a time-shift or, delay of input sequence, $x[n]$, results in a corresponding shift in the output sequence, $y[n] = \hat{T}\{x[n]\}$,

$$y[n - n_d] = \hat{T}\{x[n - n_d]\} \tag{4.3}$$

From linearity and time-invariance principles it follows that any LTI system can be completely characterized by its impulse response sequence [8,9]. Specifically, let $h[n]$ to be the response of the system to $\delta[n]$, an impulse accruing at $n = 0$, thus with,

$$\delta[n] = \begin{cases} 1, & n = 0 \\ 0, & n \neq 0 \end{cases}, \tag{4.4}$$

the impulse response is give by,

$$h[n] = \hat{T}\{\delta[n]\}. \tag{4.5}$$

Using linearity and time-invariance of the system, one may write,

$$y[n] = \hat{T}\{x[n]\} = \hat{T}\left\{\sum_{k=-\infty}^{\infty} x[k]\delta[n-k]\right\} = \sum_{k=-\infty}^{\infty} x[k]\hat{T}\{\delta[n-k]\}$$
$$= \sum_{k=-\infty}^{\infty} x[k]h[n-k] \tag{4.6}$$

A system is said to be *causal* if the output of the system at any time n depends only on present and past inputs (i.e., $x[n]$, $x[n\text{-}1]$, $x[n\text{-}2]$,...), but does not depend on future inputs (i.e., $x[n+1]$, $x[n+2]$,...). Otherwise the system is called *noncausal*. It is apparent that in real-time signal processing applications, future values of the signal cannot be observed and hence, noncausal system is physically unrealizable. Causality of a LTI system can be expressed in terms of its impulse response as,

$$h[n] = 0, \quad \text{for } n < 0. \tag{4.7}$$

Equation (4.6) is commonly called the *convolution sum* or simply the convolution. Convolution of two sequences is defined as,

$$x_1[n] * x_2[n] = \sum_{k=-\infty}^{\infty} x_1[k]x_2[n-k]. \tag{4.8}$$

With the definition (4.8), equation (4.6) can be represented by the notation

$$y[n] = \hat{T}\{x[n]\} = x[n] * h[n] \tag{4.9}$$

Using definition (4.8) it is easy to verify the following properties of convolution:

commutative law

$$x_1[n] * x_2[n] = x_2[n] * x_1[n] \tag{4.10}$$

associative law

$$x_1[n] * (x_2[n] * x_3[n]) = (x_1[n] * x_2[n]) * x_3[n] \tag{4.11}$$

distributive law

$$h[n]*\left(x_1[n]+x_2[n]\right)=h[n]*x_1[n]+h[n]*x_2[n] \tag{4.12}$$

From commutative property it follows that the output of two LTI systems in cascade does not depend on the order in which transformations are applied, therefore,

$$\hat{T}_1\left\{\hat{T}_2\left\{x[n]\right\}\right\}=\hat{T}_2\left\{\hat{T}_1\left\{x[n]\right\}\right\}. \tag{4.13}$$

Distributive property implies that the cascade of two LTI systems with impulse response, $h_1[n]$, $h_2[n]$, is also equivalent to a LTI system with an impulse response, $h[n]$, given by,

$$h[n]=h_1[n]*h_2[n]. \tag{4.14}$$

4.2 Z-transform Definition

The Z-transform $X(z)$ of a discrete-time sequence $x[n]$ is a function of complex variable, z, and defined as the power series, such that,

$$X(z)=\sum_{n=-\infty}^{\infty}x[n]z^{-n}. \tag{4.15}$$

Z-transform defined by (4.15) can be considered as an operator that transforms a discrete sequence into a function of complex variable z. The correspondence between a sequence and its Z-transform is indicated by the notation

$$x[n]\overset{Z}{\longleftrightarrow}X(z). \tag{4.16}$$

Region of convergence (ROC) of power series (4.15) is given by $0\le r_1<|z|<r_2\le\infty$ [21]. Since, the impulse response of a causal system (4.7) is one-sided, it follows that ROC of its Z-transform is the exterior of some circle $r<|z|$. Definition of Z-Transform can be

considered also as *Laurent* series expansion of $X(z)$ [21]. This interpretation can be helpful when inverting Z-transform, i.e. reconstructing discrete sequence from its Z-Transform.

Z-transform of LTI system's impulse response, $h[n]$, is called *system transfer function* and plays an important role in the analysis of LTI systems:

$$H(z) = \sum_{n=-\infty}^{\infty} h[n] z^{-n}. \tag{4.17}$$

With $z = e^{j\omega}$ the Z-transform (4.15) becomes

$$X(e^{j\omega}) = \sum_{n=-\infty}^{\infty} x[n] e^{j\omega n} \tag{4.18}$$

which is the Fourier transform of the sequence $x[n]$ (*see Section* 4.6).

Z-transform has many useful properties when studding discrete-time signals and systems [8,9]. The most important properties are linearity, time shifting and convolution. If given are two sequences with their Z-transforms $x_1[n] \overset{Z}{\longleftrightarrow} X_1[z]$ and $x_2[n] \overset{Z}{\longleftrightarrow} X_2[z]$ then, the above mentioned properties can be formulated as,

linearity

$$x[n] = a_1 x_1[n] + a_2 x_2[n] \overset{Z}{\longleftrightarrow} X(z) = a_1 X_1(z) + a_2 X_2(z) \tag{4.19}$$

for any constants a_1 and a_2;

time-shifting law

if $x[n] \overset{Z}{\longleftrightarrow} X(z)$ then

$$x[n-k] \overset{Z}{\longleftrightarrow} z^{-k} X(z); \tag{4.20}$$

convolution law

$$x_1[n] * x_2[n] \xleftrightarrow{Z} X_1(z)X_2(z) \tag{4.21}$$

Convolution property allows to establish a relation between Z-transforms of the input $x[n]$ and output $y[n]$ sequences of the LTI system: applying relation (4.21) to equation (4.9) and recalling the definition of system transfer function (4.17), it can be shown that Z-transform of output sequence $Y(z)$ is given by,

$$Y(z) = H(z)X(z) \tag{4.22}$$

Other important properties

linearity,

$$a_1 x_1[n] + a_2 x_2[n] \xleftrightarrow{Z} a_1 X_2[n] + a_2 X_2[n], \tag{4.23}$$

and *time-shifting,*

$$x[n-n_0] \xleftrightarrow{Z} z^{-n_0} X(z), \tag{4.24}$$

can be easily derived using the definition of Z-transform.

4.3 Rational Transfer Function Systems

Consider a LTI system described by the difference equation with constant coefficients,

$$y[n] = -\sum_{k=1}^{N} a_k y[n-k] + \sum_{k=0}^{M} b_k x[n-k]. \tag{4.25}$$

Z-transforming both sides of (4.25) and using linearity (4.24) and time-shift (4.24) properties, one arrives at

$$\left(1 + \sum_{k=1}^{N} a_k z^{-k}\right) Y(z) = \left(\sum_{k=0}^{M} b_k z^{-k}\right) X(z). \tag{4.26}$$

Comparing (4.22) and (4.26) it can be concluded that the system defined by the difference equation (4.25) has a rational transfer function,

$$H(z) \equiv \frac{B(z)}{A(z)} = \frac{b_0 + b_1 z^{-1} + \ldots + b_M z^{-M}}{1 + a_1 z^{-1} + \ldots + a_N z^{-N}}. \tag{4.27}$$

An important property of rational transfer function systems is that they can be implemented using only finite number of shift register.

4.4 One-sided Z-transform

Transformation defined by (4.15) is also referred to as *two-sided* or, *bilateral* Z-transform. It requires the discrete-time signal to be specified for the entire time range, $-\infty < n < \infty$. This requirement prevents its use for solving initial value problems, when the input signal is known only at a finite time point. One-sided Z-transform is best suited for this class of problems. It is defined as,

$$\begin{aligned} x[n] &\xleftrightarrow{Z^+} X^+(z) \equiv Z^+\{x[n]\} \\ X^+(z) &\equiv \sum_{n=0}^{\infty} x[n] z^{-n}. \end{aligned} \tag{4.28}$$

One-sided Z-transform differs from two-sided transform in the lower limit of the summation; in one-sided transform it is always zero, whether or not the signal is zero for $n<0$. Almost all properties of two-sided Z-transform may be carried over to a one-sided transformation with exception of time-shifting property [8]. Using definition (4.28) it can be shown for a delayed sequence, $k>0$, that,

$$Z^+\{x[n-k]\} = z^{-k}\left[\sum_{l=-k}^{-1} x[l] z^{-l} + \sum_{l=0}^{\infty} x[l] z^{-l} + \right] = z^{-k}\left[\sum_{n=1}^{k} x[-n] z^{n} + X^+(z)\right]. \tag{4.29}$$

Similarly, one-sided Z-transform of time-advanced sequence is given as,

$$Z^+\{x[n+k]\} = z^{k}\left[-\sum_{n=0}^{k-1} x[n] z^{-n} + X^+(z)\right], \quad k>0. \tag{4.30}$$

Let us evaluate the response of a system which is defined by recursive finite difference (4.25) to a signal $x[n]$ applied at $n = 0$. The effect of all previous input is reflected in the initial conditions $y(-1), y(-2), \ldots, y(-N)$. Using the time-shift property (4.29), one-sided Z-transform of (4.25) becomes,

$$Y^+(z) = -\sum_{k=1}^{N} a_k z^{-k} \left[Y^+(z) + \sum_{n=1}^{k} y(-n) z^n \right] + \sum_{k=0}^{M} b_k z^{-k} X^+(z). \tag{4.31}$$

Since it is assumed that the signal $x[n] = 0$ for $n<0$, one-sided and two-sided Z-transforms are identical, $X^+(z) = X(z)$. From (4.31) it follows that one-sided Z-transform of the output sequence will be given by,

$$Y^+(z) = H(z)X(z) + \frac{N_0(z)}{A(z)}, \tag{4.32}$$

where $A(z)$ is the denominator of $H(z)$ as defined by (4.27) and,

$$N_0(z) = -\sum_{k=1}^{N} \left(a_k z^{-k} \sum_{n=1}^{k} y(-n) z^n \right). \tag{4.33}$$

The first term of the right hand side of (4.32) is due to the input signal only and referred to as, zero-state response. The second term is due to the initial conditions and referred to as, zero-input response [22]

4.5 Stability of LTI systems

Stability is an important property that must be considered in any practical implementation of discrete-time systems. A discrete-time system is stable in bounded-input, bounded-output sense (BIBO) if and only if, every bounded sequence produces a bounded output sequence. For a LTI systems, BIBO stability is equivalent to *absolute* summability of its impulse response [8,9],

$$\sum_{k=-\infty}^{\infty} |h[k]| < \infty . \tag{4.34}$$

Equation (4.34) for LTI systems implies that the system's transfer function, $H(z)$ must contain the unit circle within its ROC: if $|z| = 1$, then, from (4.34) it follows that,

$$|H(z)| \le \sum_{n=-\infty}^{\infty} |h(n) z^{-n}| = \sum_{n=-\infty}^{\infty} |h(n)| < \infty \tag{4.35}$$

For a causal system the condition of stability can be narrowed to some extent. Indeed, a causal system is characterized by a system transfer function $H(z)$ having as a ROC the exterior of some unit circle of radius r. For a stable system, ROC must include the unit circle. Therefore, it follows that *a causal linear time-invariant system is BIBO stable, if and only if, all poles of its system transfer function are inside the unit circle*.

4.6 The Fourier Transform of Discrete-Time Signals

Fourier transform of a discrete time-sequence is defined as

$$X(e^{j\omega}) = \sum_{n=-\infty}^{\infty} x[n] e^{-j\omega n} \tag{4.36}$$

As it was pointed out above, according to (4.18) Fourier transform can be interpreted as the Z-Transform, $x[n] \overset{Z}{\longleftrightarrow} X(z)$, evaluated on the unit circle, $z = e^{j\omega}$, which may also explains the choice of argument for Fourier transform as, $e^{j\omega}$,in (4.36).

For a very wide class of sequences, Fourier transform can be inverted to reconstruct discrete sequence,

$$x[n] = \frac{1}{2\pi} \int_{-\pi}^{\pi} X(e^{j\omega}) e^{j\omega n} d\omega . \tag{4.37}$$

Fourier transform of $h(n)$, $H\left(e^{j\omega}\right)$, also referred to as frequency response of LTI, plays an important role in the analysis of discrete-time systems and signals. From the equation (4.22) and the fact that the Fourier transform is Z-transform evaluated on the unit circle, it follows immediately that,

$$Y\left(e^{j\omega}\right) = H\left(e^{j\omega}\right) X\left(e^{j\omega}\right), \tag{4.38}$$

which relates the Fourier transform of input sequence to the Fourier transform of the output sequence.

4.7 Discrete-Time Differentiator

Let us be given samples of continuous-time signal $x[n] = f(n\Delta t)$ and its derivative, $y[n] = f'(n\Delta t)$. They can be thought as the input and output of LTI system,

$$y[n] = \hat{T}\{x[n]\}. \tag{4.39}$$

If continuous-time function is bandlimited and conditions of Nyquist sampling theorem [8,9] are met, then, the discrete-time differentiator (4.39) is uniquely defined. To determine its frequency response, $H\left(e^{j\omega}\right)$, let us assume that the continuous-time sequence is harmonic $f(t) = e^{j\Omega t}$. Its samples are, $x[n] = e^{j\Omega\Delta tn}$; samples of derivative are given by, $y[n] = j\Omega e^{j\Omega\Delta tn}$. Comparing these expressions with frequency response property (4.38) immediately leads to,

$$H\left(e^{j\omega}\right) = j\frac{\omega}{\Delta t}. \tag{4.40}$$

Similarly, it can be shown that the frequency response of a second order time-differentiator, $y[n] = f''(n\Delta t)$ is given by,

$$H\left(e^{j\omega}\right) = -\frac{\omega^2}{\Delta t^2}. \tag{4.41}$$

From the inversion formula (4.37) is follows that discrete-time systems, defined by their frequency response (4.40) and (4.41), have their impulse response sequence provided in $-\infty$ to ∞. This means that the input signal must be known for all times, in order to compute the output. Therefore, these systems are not physically realizable in real-time applications. Sub-optimal approximation of ideal differentiators, as defined by (4.40) and (4.41), are considered in the following chapter.

CHAPTER 5

Z-TRANSFORM ANALYSIS OF FDTD TIME-STEPPING

5.1 Differentiator Approximation

Z-Transform theory has been employed by Sullivan [23] to implement frequency dependant materials into FDTD modeling. By sampling and then Z-Transforming time-domain relaxation function of frequency dependant medium, convolution integral has been interpreted as a discrete-time rational transfer function system, which could be readily implemented as a recursive finite-difference scheme with constant coefficients. This approach allowed straightforward implementation of many dispersive materials into FDTD modeling. Following the work by Weedon and Rappaport [24] further extended capabilities of the technique. In contrast to Sullivan's approach, method [24] did not use analytical relaxation function of the medium, which may not be known in may practical situations; instead, Weedon and Rappaport proposed to approximate directly experimental data in the frequency band of interest.

In Section 2.4 simple examples of time-domain discretization were described. In this section, a more general approximation of the time-derivative operator is considered. Central difference approximation of time-derivative of Yee's algorithm (1.1) is replaced here by a discrete-time LTI system. This approach is similar to the above mentioned techniques in order to incorporate frequency dispersive materials into FDTD modeling. While the media are assumed to be nondispersive; the time-derivatives itself are the source of frequency dispersion.

Frequency response of first-and second-order differentiators are given by (4.40) and (4.41). Any discrete-time system, which is meant to perform as a differentiator, should conform to the frequency response of (4.40) or, (4.41), in the frequency band of interest, $\omega_{\min} \le \omega \le \omega_{\max}$. The first order differentiator (4.40) is used to discretize coupled Maxwell's equations (2.1), (2.2) for the electric and magnetic fields, whereas, the second order (2.2) differentiator is used to discretize uncoupled vector wave equation for electric (2.13) and magnetic (2.12) fields.

Spatial discretization of Maxwell's equations for lossless isotropic medium (2.1) and (2.2) can be written in matrix form as,

$$\begin{bmatrix} \mu\dfrac{\partial}{\partial t} & 0 \\ 0 & \varepsilon\dfrac{\partial}{\partial t} \end{bmatrix} \begin{bmatrix} H \\ E \end{bmatrix} = \begin{bmatrix} 0 & -D_E \\ D_H & 0 \end{bmatrix} \begin{bmatrix} H \\ E \end{bmatrix} + \begin{bmatrix} S_1 \\ S_2 \end{bmatrix}, \tag{5.1}$$

where, S_1, S_2, account for external sources, D_E and D_H implement **curl** transform in a discrete form and operate on electric and magnetic fields, respectively. For a lossless medium, the permittivity, ε, and the permeability, μ, matrices are diagonal and positively defined. Time-domain discretization of (5.1) is performed as follows,

$$y[n] \equiv \frac{1}{\delta t}\hat{T}\{x[n]\} \approx \left.\frac{\partial x(t)}{\partial t}\right|_{t=n\delta t} \tag{5.2}$$

$$y[n] = \frac{1}{\delta t}\sum_{k=0}^{M} b_k x[n-k] - \sum_{k=1}^{N} a_k y[n-k] \tag{5.3}$$

where, δt, is the time-step, a_k and b_k are constants. Equation (5.3) can be thought as a generalization of simple central difference approximation,

$$y[n] \equiv \frac{1}{\delta t}\left\{x\left((n+1/2)\delta t\right) - x\left((n-1/2)\delta t\right)\right\} \approx \left.\frac{\partial x}{\partial t}\right|_{t=n\delta t}. \tag{5.4}$$

As discussed in Section 4.3, the discrete-time system defined by (5.3) has a rational function Z-Transform,

$$T(z)=\frac{B(z)}{A(z)}=\frac{b_0+b_1z^{-1}+\ldots+b_Nz^{-M}}{1+a_1z^{-1}+\ldots+a_Nz^{-N}}. \tag{5.5}$$

With time-discretization according to (5.2), fully discretized Maxwell's equation are given as,

$$\frac{1}{\delta t}\begin{bmatrix}\mu\hat{T}_H & 0\\ 0 & \varepsilon\hat{T}_E\end{bmatrix}\begin{bmatrix}H^n\\ E^n\end{bmatrix}=\begin{bmatrix}0 & -D_E\\ D_H & 0\end{bmatrix}\begin{bmatrix}H^n\\ E^n\end{bmatrix}+\begin{bmatrix}S_1^n\\ S_2^n\end{bmatrix} \tag{5.6}$$

where, $\hat{T}_H$, $\hat{T}_E$, operate on the magnetic and electric fields, respectively.

5.2 Stability Condition

Taking one-sided Z-Transform of (5.6) as it is discussed in Section 4.4 leads to,

$$\begin{bmatrix}\frac{1}{\delta t}B_H(z)\mu & A_H(z)D_E\\ -A_E(z)D_H & \frac{1}{\delta t}B_E(z)\varepsilon\end{bmatrix}\begin{bmatrix}H(z)\\ E(z)\end{bmatrix}=\begin{bmatrix}A_H(z)S_1(z)\\ A_E(z)S_2(z)\end{bmatrix}-\frac{1}{\delta t}\begin{bmatrix}\mu N_1(z)\\ \varepsilon N_2(z)\end{bmatrix} \tag{5.7}$$

where the terms, $N_1(z), N_2(z)$, are the result of the initial conditions for the causal filters, $\hat{T}_H, \hat{T}_E$, in accordance to (4.33). They are finite order polynomials and do not have poles outside of the unit circle and therefore, do not affect the stability of the algorithm. In practical applications, external sources do not grow exponentially with the number of time-steps therefore, their Z-Transforms, $S_1(z)$ and $S_2(z)$, do not have poles outside the unit circle, $|z|>1$. Since the right hand side of (5.7) does not contain poles for $|z|>1$ it can be concluded that an *FDTD algorithm, which is defined by the finite-difference equations* (5.6)*, is stable if and only if the determinant of the set of linear equations* (5.7)

does not have zeros outside the unit circle. Denoting the square matrix on the left-hand side of (5.7) by G, the stability condition can be expressed as,

$$\det(G(z)) \equiv \det\left(\begin{bmatrix} \frac{1}{\delta t}B_H(z)\mu & A_H(z)D_E \\ -A_E(z)D_H & \frac{1}{\delta t}B_E(z)\varepsilon \end{bmatrix}\right) \neq 0, \quad \text{for } |z| > 1. \tag{5.8}$$

If the determinant of $G(z)$ is zero for a particular value of $z = z_0$ then, there exists a nontrivial solution of homogeneous set of equations,

$$\begin{bmatrix} \frac{1}{\delta t}B_H(z_0)\mu & A_H(z_0)D_E \\ -A_E(z_0)D_H & \frac{1}{\delta t}B_E(z_0)\varepsilon \end{bmatrix}\begin{bmatrix} H_0 \\ E_0 \end{bmatrix} = 0. \tag{5.9}$$

Eliminating H_0, from (5.9) results in

$$\left[\delta t^2 A_E(z_0)A_H(z_0)B_H^{-1}(z_0)D_H\mu^{-1}D_E + B_E(z_0)\varepsilon\right]E_0 = 0. \tag{5.10}$$

For (5.10) to have a non-trivial solution, the determinant of system of equations must be zero,

$$\begin{aligned} &\det\left(\delta t^2 A_E(z_0)A_H(z_0)B_H^{-1}(z_0)D_H\mu^{-1}D_E + B_E(z_0)\varepsilon\right) \\ &= \det(\varepsilon)\det\left(c^2\delta t^2 \frac{A_E(z_0)A_H(z_0)}{B_H(z_0)}\varepsilon_r^{-1}D_H\mu_r^{-1}D_E + B_E(z_0)\right) = 0, \end{aligned} \tag{5.11}$$

where, $c = (\varepsilon_0\mu_0)^{-\frac{1}{2}}$ is the speed of light and, $\varepsilon = \varepsilon_0\varepsilon_r$, $\mu = \mu_0\mu_r$. Since, $\det(\varepsilon) \neq 0$ equation (5.11) can be rewritten as,

$$\prod_l \left(T_H(z_0)T_E(z_0) + c^2\delta t^2\lambda_l\right) = 0, \tag{5.12}$$

where, λ_l is an eigenvalue of $\varepsilon_r^{-1}D_H\mu_r^{-1}D_E$ and multiplication in (5.12) is carried out over all eigenvalues. The range of eigenvalues λ_l must be determined and the transfer

functions in (5.12) be chosen accordingly, in order to ensure stability of the algorithm. Let us apply criteria (5.12) to the central difference approximation (5.4). The electric and magnetic fields are staggered in time, therefore,

$$\begin{aligned} H^n &= H((n-\frac{1}{2})\delta t) \\ E^n &= E(n\delta t). \end{aligned} \tag{5.13}$$

Using (5.4) and (5.13) FDTD equations are given by,

$$\begin{aligned} \frac{H^{n+1}-H^n}{\delta t} &= -\mu^{-1}D_E E^n \\ \frac{E^{n+1}-E^n}{\delta t} &= \varepsilon^{-1}D_H H^{n+1} \end{aligned} \tag{5.14}$$

which is equivalent to (5.6) with no external sources. Corresponding transfer functions are given by,

$$T_H(z) = z - 1 \tag{5.15}$$

$$T_E(z) = 1 - z^{-1}. \tag{5.16}$$

For the time-stepping (5.14) to be stable it is required that none of the product terms in (5.12) can be zero outside the unit circle,

$$z\left(1-z^{-1}\right)^2 + c^2\delta t^2\lambda_\eta \neq 0, \quad |z| > 1 \tag{5.17}$$

Substitution of $z = e^{j\omega}$ into (5.17) leads to,

$$\sin^2\left(\frac{\omega}{2}\right) - \frac{1}{4}\cdot c^2\delta t^2\lambda_\eta \neq 0. \tag{5.18}$$

Recalling that ω must be real, it can be concluded from (5.18) that the time-stepping (5.14) is stable for all eigenvalues λ_η of $\varepsilon_r^{-1}D_H\mu_r^{-1}D_E$, if, the following inequality holds:

$$0 \leq \frac{1}{4}\cdot c^2\delta t^2\lambda_\eta \leq 1. \tag{5.19}$$

For the general case of irregular unstructured grid, it may not be possible to establish the range of eigenvalues λ_i in (5.19) and hence the stability limit, $\delta t_{\max}$. However, through numerical experimentation, a simple relationship has been established that provides an excellent estimate of the time-step bound for tetrahedral, pentahedral and hexahedral elements [16],

$$\delta t_{\max} \leq \frac{1}{c \sup\left(\sqrt{\sum_{i=1}^{3} \frac{1}{l^2}}\right)}, \tag{5.20}$$

where, $l_i (i = 1,3)$ are three edges in each cell sharing a common vertex. This expression provides a bound on the time step, which is within 10% of actual stability limit. From (5.19) and (5.20) it follows that

$$0 \leq \lambda_{\max} \leq 4 \sup\left(\sum_{i=1}^{3} \frac{1}{l_i^2}\right). \tag{5.21}$$

Inequality (5.21) should be interpreted as an empirical bound on the eigenvalues of $\varepsilon_r^{-1} D_H \mu_r^{-1} D_E$. With (5.21) the stability bound (5.12) can be restated as,

$$T_H(z) T_E(z) + C \neq 0, \tag{5.22}$$

for any $|z| > 1$ and any possible values of the parameter C such that,

$$0 \leq C \leq 4c^2 \delta t^2 \sup\left(\sum_{i=1}^{3} \frac{1}{l_i^2}\right). \tag{5.23}$$

It is shown below, that for a given choice of transfer functions, there is an upper bound C_{max} on the parameter C, for which (5.22) holds true for any $|z| > 1$. Hence, from (5.23) the time-step bound is given by,

$$\delta t_{\max} \le \frac{C_{\max}^{1/2}}{2c \sup\left(\sqrt{\sum_{i=1}^{3} \frac{1}{l_i^2}}\right)} \tag{5.24}$$

In the following, a transfer function that which minimizes the approximation error is presented.

Let us consider special choice of transfer functions,

$$F(z) \equiv -T_H(z)T_E(z) = -|Q|^2 P(z)\left(P(1/z^*)\right)^*, \tag{5.25}$$

where, $P(z)$ is the rational function i.e. ratio of two polynomials of z^{-1}, which can be written as,

$$P(z) = \frac{\prod_{i=1}^{K}(1 - r_i z^{-1})}{\prod_{j=1}^{L}(1 - p_j z^{-1})} \tag{5.26}$$

Choice (5.25) guaranties that $F(z)$ is positive on the unit circle, $z = e^{j\omega}$, $0 \le \omega \le 2\pi$, which is desirable since, the parameter C in (5.22) is also positive. Other possible choices are considered in Chapter 6. The constant Q in (5.25) and zeros and poles of $P(z)$ in (5.26) should be chosen so that *in the frequency range of interest*, $F\left(e^{j\omega}\right)$ matches the normalized frequency response of ideal differentiator (4.41), namely,

$$F(e^{j\omega}) \approx \omega^2, \ \omega_{\min} \le \omega \le \omega_{\max}. \tag{5.27}$$

The number of roots of the following equation,

$$-T_H(z)T_E(z) = F(z) = C, \tag{5.28}$$

is equal to the order of rational function $F(z)$. All roots of (5.28) are located on the unit circle if the order of numerator of $F(z)$ is not less than the order of its denominator, i.e. $K \ge L$ in (5.26), and all zeros of $P(z)$ are located on the unit circle. The validity of the

preposition is easier to understand considering examples discussed in the next section. Also, Appendix A discusses another way to identify transfer functions suitable for stable time-marching.

5.3 Transfer function Examples

Explicit scheme. Let us consider a transfer function, which is defined by,

$$P(z)=\left(1-z^{-1}\right)\frac{1-rz^{-1}}{1-pz^{-1}} \tag{5.29}$$

and results in,

$$T_H(z)=Q(1-z)\frac{1-r^*z}{1-p^*z}=-\frac{Q}{p^*}\frac{r^*z-(1+r^*)z^0+z^{-1}}{1-p^{*-1}z^{-1}} \tag{5.30}$$

$$T_E(z)=Q^*(1-z^{-1})\frac{1-rz^{-1}}{1-pz^{-1}}=Q^*\frac{z^0-(1+r)z^{-1}+rz^{-2}}{1-pz^{-1}}. \tag{5.31}$$

From (5.30) it is easy to see that the approximation of time-derivative according to (5.3) results in a magnetic field, which is one step ahead of the electric field. Therefore, the time-stepping defined by (5.29) is fully explicit with the magnetic field being one step ahead of the electric field.

Good results in many practical applications can be obtained with a grid size which is of 1/20 of the minimum significant wavelength of spectral component. The time-step bound of conventional FDTD is $\delta t_{\max}=\Delta/(c\sqrt{N})$. Therefore, the normalized frequency of minimum wavelength spectral component is $f_{\max}=1/(20\sqrt{3})=0.0289$ for 3D problems and $f_{\max}=1/(20\sqrt{2})=0.0354$ for 2D problems. It was found empirically [36] that by choosing (also see appendix),

$$r = e^{j0.22\pi}$$
$$p = 0.999e^{j0.219\pi} \tag{5.32}$$
$$Q = 0.9949e^{j0.09464}$$

in (5.30) and (5.31), time-sampling error was significantly reduced in the frequency interval $0 \le f \le f_{\max}$. Figure 5.1 shows the normalized error $(\omega^2 - F(e^{j\omega}))/\omega^2$ of the

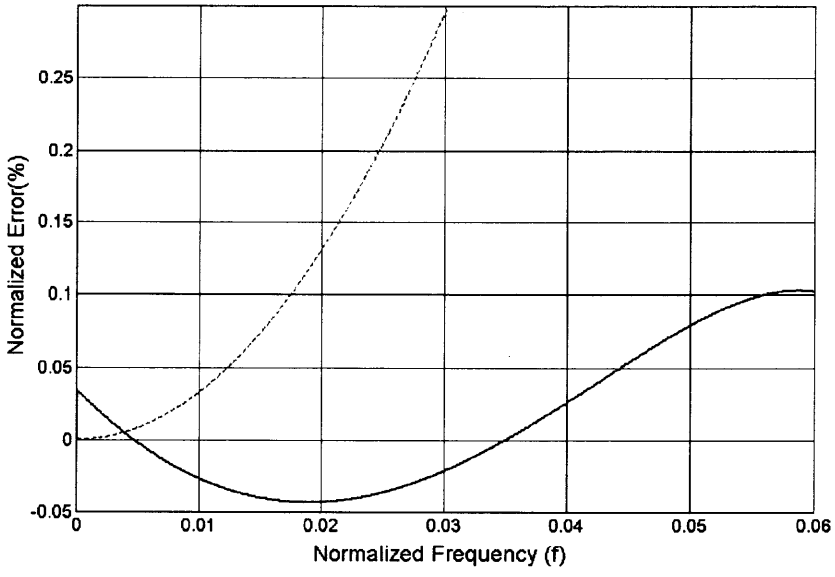

Figure 5.1 Time sampling error for the transfer function defined by (5.32) (solid line) and error for Yee's time-discretization.

proposed and the conventional FDTD. It can be seen that in the frequency range of practical interest, the error is significantly reduced compared to the conventional FDTD and is bellow 0.05%. Note that unlike the conventional FDTD, the sampling error does not vanish at $\omega \to 0$. This is because parameters in (5.32) were chosen to reduce the sampling error at the higher frequencies. Namely, the accuracy of the algorithm at lower frequencies is deliberately sacrificed, though slightly, for the purpose of better performance at higher frequencies. Stability bound of the time-stepping can be deduced from Figure 5.2. With $F(z)$ defined by (5.25) and (5.29), equation (5.28) becomes a fourth

order polynomial equation and therefore, has no more than four distinct roots for any value of C. From Figure 5.2 it can be seen that any horizontal line $0 < y = C < C_{\max} = 3.96$ will cross the plot of $F(e^{j\omega})$ exactly four times. Therefore, all roots of (5.28) are located on the unit circle $|z| = 1$ and stability condition (5.22) is satisfied for all $|z| > 1$. From (5.15) and (5.16), it can be derived that for the conventional FDTD, the analogues parameter, $C_{max} = 4$, and from (5.24), it follows that the stability bound of the new algorithm differs from that of a conventional FDTD by less than 1%.

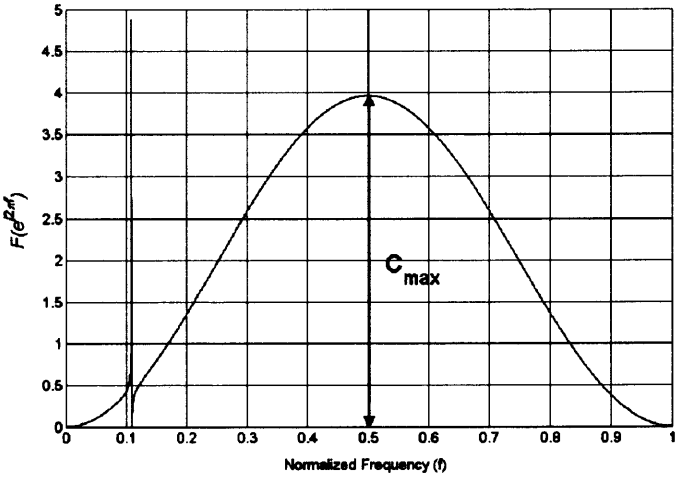

Figure 5.2 Plot of $F\left(e^{j\omega}\right)$ defined by (5.32)

Implicit scheme. Time step of implicit FDTD is not limited by the stability requirement, rather, it should be chosen to ensure algorithm accuracy. Since the computational burden required to update fields into the next time-step is much larger here in comparison with an explicit algorithm, it is desired to operate an implicit FDTD at large time-steps. By manipulating the coefficients of (5.26) it was found [36] that the following choice leads to a transfer function with desired properties:

$$P(z)=\frac{1-e^{j\pi 0.129}z^{-1}}{1-e^{j\pi 1.686}z^{-1}},$$
$$Q=2.8385e^{j0.8749} \tag{5.33}$$

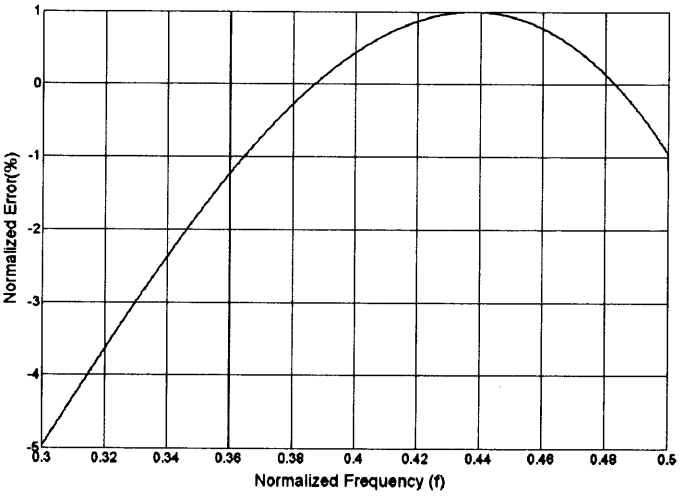

Figure 5.3 Time-sampling error for implicit scheme defined by (5.33)

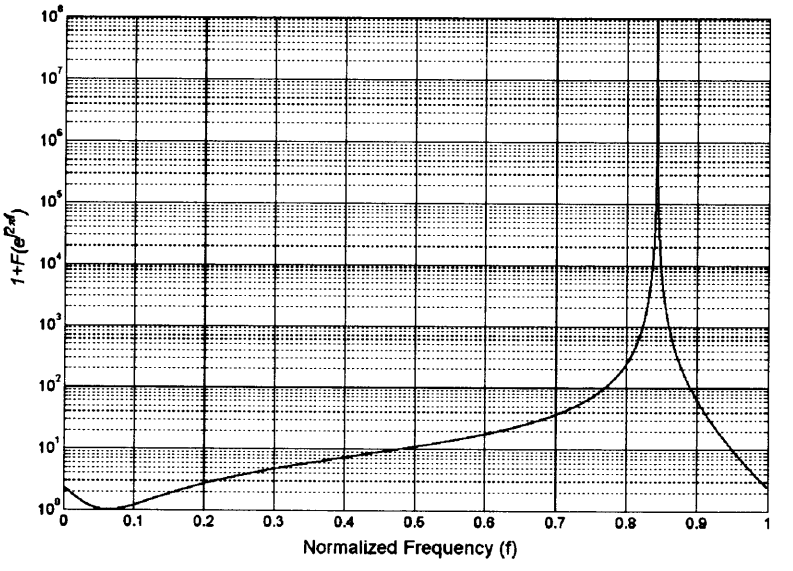

Figure 5.4 Plot of $F\left(e^{j\omega}\right)$ defined by (5.33)

From Figure 5.3 it can be seen that the time-sampling error is below 1% for $0.37 \le f \le 0.5$, which close to the limit allowed by Nyquist sampling theorem [8,9]. Highest possible . Figure 5.4 shows a plot of the transfer function on the unit circle. Since $P(z)$ has a pole on the unit circle, $C_{\max} = \infty$, and the algorithm is unconditionally stable.

5.4 Implementation

Memory efficient implementation of time-stepping (5.6) can be achieved by using direct form II structure for recursive finite-difference equation (5.3) [8,9]. The system with the transfer function (5.5) ($a_0 = 1$) can be viewed as two cascaded transforms, namely, an all-pole system with a transfer function, $\frac{1}{A(z)}$,

$$w[n] = -\sum_{k=1}^{N} a_k w[n-k] + x[n], \tag{5.34}$$

and an all-zero system with the transfer function $B(z)$,

$$y[n] = \sum_{k=0}^{M} b_k w[n-k]. \tag{5.35}$$

As an example, let us derive the update-equations for the explicit case

$$T_H(z) = zT_E(z) = \frac{z\left(b_0 + b_1 z^{-1} + \ldots + b_N z^{-M}\right)}{a_0 + a_1 z^{-1} + \ldots + a_N z^{-N}}. \tag{5.36}$$

The update-equation are obtained by substituting a direct form II implementation of the time-differentiators (5.34), (5.35) into (5.6) to get,

$$\frac{1}{\delta t}\hat{T}\left\{H^n\right\} = \frac{1}{\delta t}\sum_{k=0}^{M} b_k W_H^{n-k+1} = \mu^{-1}\left(-D_E E^n + S_1^n\right) \tag{5.37}$$

$$H^n = W_H^n + \sum_{k=1}^{N} a_k W_H^{n-k} \tag{5.38}$$

$$\frac{1}{\delta t}\hat{T}\left\{E^n\right\} = \sum_{k=0}^{M} b_n W_E^{n-k} = \varepsilon^{-1}\left(\hat{D}_H H^n + S_2^n\right) \tag{5.39}$$

$$E^n = W_E^n + \sum_{k=1}^{N} a_k W_E^{n-k} . \tag{5.40}$$

If all variables up to a time-step n_0 are known, then, $W_H^{n_0+1}$ can be found from (5.37). Once $W_H^{n_0+1}$ is known, then, all other variables are updated to a time-step n_0+1 by using (5.38), (5.39), and (5.40). In order to leapfrog the fields according to (5.37)-(5.40) , the field values at the latest, $L = \max\{M, N\}$, time-steps must be known. All fields at L initial time-steps must be self-consistent. In order to set initial condition for a multilevel scheme conventional FDTD can be used [20].

5.5 Discussion

The use of Z-transform theory in the analysis of stability and accuracy of various time-stepping schemes was considered. The generalization of time-stepping concept as a rational transfer function discrete-time transform has been developed. It has been found that by optimizing the transfer function coefficients, it was possible to greatly reduce the time sampling error. At the same time, stability of the original formulation has been preserved. Finally, memory efficient implementation of the time-stepping scheme was presented.

These advances are the first step in improving FDTD algorithms. The next step would be to employ more efficient spatial discretization [25], which may be the subject of future research.

CHAPTER 6

HYBRID TIME-STEPPING

6.1 Review of Hybrid Time-Domain Solvers

In Chapter 2, two major techniques for electromagnetics, FDTD and FEM, have been considered. It was shown that both methods have their own advantages and disadvantages. Therefore, it appears plausible to combine both methods into a hybrid solver which would have advantages of both FDTD and FEM and at the same time avoid problems inherent to each method. Such FEM-FDTD hybrids have been constructed [26,27,28,29], but all suffer from weak instabilities [30,31,32], referred to as late time growth. Accuracy and stability of the hybrids also depends on the choice of element basis functions [33]. This instability limits usefulness of the hybrid schemes, especially for modeling resonant systems.

Hybrid Time-Domain solver proposed by Rylander and Bondeson [6] was shown to be free of late time instability. It employs FDTD in large homogeneous volumes and FEM on unstructured grid around complex boundaries. The hybrid algorithm uses *vector finite elements* also called as *edge elements* as element basis functions [4]. Structured grid field time-marched explicitly using central difference approximation of time-derivative (2.41), whereas unstructured grid field updated implicitly using time-stepping scheme discussed by Lee et al [34]. Structured part of the grid has only hexahedral (rectangular) elements. Unstructured part of the grid contains tetrahedrons and pyramids serving as an interface between different types of the grid. Simple example of hybrid grid is shown in Figure 6.1. Basis functions for tetrahedral and rectangular elements are described in [4]

and those for pyramids in [35]. Only linear elements have been used. It is easy to verify that FDTD for vector wave equation [10] is equivalent to FEM with rectangular edge functions if trapezoidal integration is used to evaluate stiffness and mass matrices in (2.40).

Interface between explicitly and implicitly updated parts of the hybrid grid is shown in Figure 6.2. Edges marked by crosses are updated explicitly, whereas edges marked by circled updated implicitly. In another publication Rylander and Bondeson [7] proposed improved version of their hybrid solver. Also prove of stability in general case have been provided. Below, construction of the hybrid time-stepping [7] is described in more details.

Each element of the grid is classified as either explicit or implicit. Explicit elements are hexahedras of structured grid, while implicit elements consist of unstructured tetrahedras and interface pyramids.

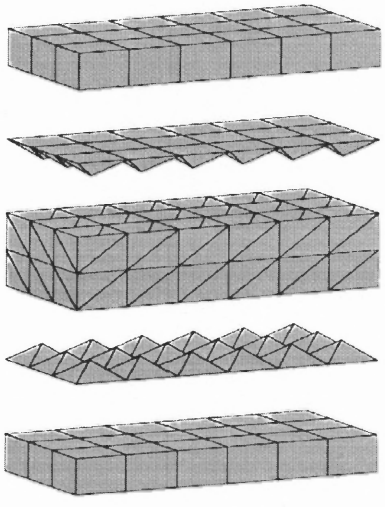

Figure 6.1 Example of simple hybrid grid
Source: Rylander, Bondeson [6]

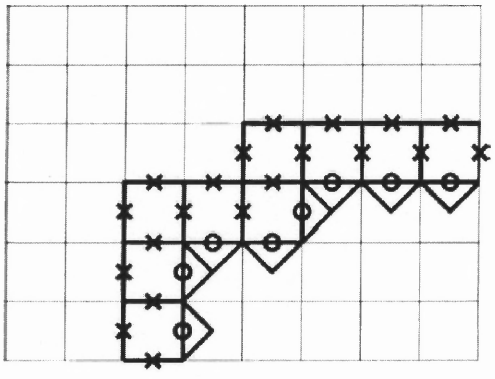

Figure 6.2 Interface between different grid types.
Source: Rylander, Bondeson [6]

Unknowns, or, degrees of freedom associated with each element depend on element classification and then, assembled into a global equation,

$$\sum_{l=1}^{K} \mathbf{S}_l \left(\theta_l \mathbf{u}^{n+1} - (2\theta_l - 1)\mathbf{u}^n + \theta_l \mathbf{u}^{n-1} \right) + \frac{1}{\delta t^2} \mathbf{M} \left(\mathbf{u}^{n+1} - 2\mathbf{u}^n + \mathbf{u}^{n-1} \right) = -\mathbf{f}^n \qquad (6.1)$$

where parameter, θ_l is chosen 0.25 or larger on the implicit elements and zero on the structured grid elements. Time-stepping (6.1) is stable up to the stability limit set by of FDTD section of the grid and given by (3.6) with, Δx, Δy, Δz, referring to the rectangular grid. Edges of rectangular elements marked by crosses in Figure 6.1 are updated explicitly using conventional FDTD time-stepping, edges marked by circles are treated as neither regular FDTD nor regular FEM. They are updated simultaneously with interior edges of the unstructured grid. It should be noted that the above discussed hybridization and prove of stability presented in [7] is not limited to the grid type depicted in Figure 6.1. Hybrid time-stepping (6.1) can be constructed for any unstructured nonuniform grid as soon as edge basis functions are available for constituting elements.

6.2 Novel Hybrid Solver with Tunable Reflection Error.

It was mentioned before that one of the drawbacks of the hybrid solver is the artificial reflection at the grid interface. The reason for the reflection is the use of different time-stepping with different types of grids. In this section, a novel technique to reduce reflection without reducing time-step is presented. The approach is based on application of Z-transform theory to analyze FDTD stability [36]. Class of transfer functions for stable hybrid time-stepping with low sampling error and low reflection error is derived. Also, rigorous proof of stability is presented for general 3D case.

Let us start by rewriting (6.1) in a more general form;

$$\sum_{l=1}^{K} \mathbf{S}_l \hat{A}_l \{\mathbf{u}^n\} + \frac{1}{\delta t^2} \mathbf{M} \hat{B} \{\mathbf{u}^n\} = -\mathbf{f}^n, \tag{6.2}$$

where, $\hat{A}_l\{...\}$, is the all-pole part of some rational transfer function system; i.e. it is represented by the denominator of (4.27) and defined by the equation,

$$\hat{A}\{\mathbf{u}^n\} = -\sum_{k=0}^{N} a_k \mathbf{u}^{n-k}. \tag{6.3}$$

Similarly, $\hat{B}\{...\}$ is the all-zero part and defined by the numerator of (4.27) according to,

$$\hat{B}\{\mathbf{u}^n\} = \sum_{k=0}^{M} b_k \mathbf{u}^{n-k}. \tag{6.4}$$

Taking one-sided Z-transform of (6.2) leads to,

$$\left[\sum_{l=1}^{K} \mathbf{S}_l A_l(z) + \frac{1}{\delta t^2} \mathbf{M} B(z)\right] \mathbf{u}(z) = -\mathbf{f}(z) + \mathbf{R}(z) \tag{6.5}$$

In (6.5) the term $\mathbf{R}(z)$ is the polynomial of z and accounts for initial conditions. If external sources do not grow exponentially with number of time-steps, term $\mathbf{f}(z)$ does not have poles outside the unit circle. Time-stepping (6.2) is stable if the formal solution of (6.5) $\mathbf{u}(z)$ does not have poles outside the unit circle. Therefore, coefficients of $A_l(z)$ and $B(z)$ in (6.5) need to be chosen so that the determinant of the system (6.5) does not have zeros outside the unit circle, or,

$$\det\left(\sum_{l=1}^{K} \mathbf{S}_l A_l(z) + \frac{1}{\delta t^2} \mathbf{M} B(z)\right) \neq 0, \quad |z| > 1. \tag{6.6}$$

If (6.6) does not hold for some $|z_0| > 1$, then, there exists a nontrivial solution of homogeneous system,

$$\left[\sum_{l=1}^{K} \mathbf{S}_l A_l(z_0) + \frac{1}{\delta t^2} \mathbf{M} B(z_0)\right] \mathbf{u}_0 = 0. \tag{6.7}$$

Multiplying (6.7) by complex transpose of $\mathbf{u}_0$, gives us,

$$\sum_{l=1}^{K} \mathbf{u}_0^H \mathbf{S}_l \mathbf{u}_0 A_l(z_0) + \frac{1}{\delta t^2} \mathbf{u}_0^H \mathbf{M} \mathbf{u}_0 B(z_0) = 0 \tag{6.8}$$

In order for time-stepping (6.2) to be stable, finite difference coefficients in (6.3) and (6.4) need to be chosen so that (6.8) cannot hold true for $\mathbf{u}_0 \neq 0$. At the same time, time-stepping accuracy is achieved if the discrete time-system defined by its transfer function $T(z) = B(z)/A(z)$ is a good approximation of second order time differentiator within the *numerical* frequency band of interest, $\omega_{\min} < \omega < \omega_{\max}$,

$$T\left(e^{j\omega}\right) \approx -\omega^2 \tag{6.9}$$

In the next section class of transfer functions for stable and low error operation is derived.

5.3 Proof of Stability and Transfer function Optimization

In this section procedure to design transfer function according to requirements (6.6) and (6.9) is presented. Let us start with pole-zero representation of the transfer function,

$$T(z) = \frac{\prod_{i=1}^{M}\left(1 - r_i z^{-1}\right)}{Q z^{-L} \prod_{i=1}^{N}\left(1 - p_i z^{-1}\right)}, \quad L, M, N \geq 0. \tag{6.10}$$

For reasons explained below, it desirable that zeros $r_i = e^{j\phi_i}$ and poles $p_i = e^{j\psi_i}$ to be located on the unit circle. Setting $z = e^{j\omega}$ in (6.10) gives us the following relation,

$$T(e^{j\omega}) = \frac{(-2j)^{M-N}}{Q} \exp\left\{\frac{j}{2}\left(\sum_{i=1}^{M}\phi_i - \sum_{i=1}^{N}\psi_i\right)\right\} \times \exp\left\{\frac{j\omega}{2}(2L + N - M)\right\} \frac{\prod_{i=1}^{M}\sin\left(\frac{\phi_i - \omega}{2}\right)}{\prod_{i=1}^{N}\sin\left(\frac{\psi_i - \omega}{2}\right)}. \tag{6.11}$$

Because of (6.9), the frequency dependant phase factor in (6.11) should vanish; this leads to,

$$M - N = 2L . \tag{6.12}$$

Also, the phase factor contributed by zeros and poles should be canceled by phase of Q, therefore,

$$Q = \pm |Q| \exp\left\{ \frac{j}{2} \left(\sum_{i=1}^{M} \phi_i - \sum_{i=1}^{N} \psi_i \right) \right\}. \tag{6.13}$$

If (6.9) is required to hold for small frequencies, then, the transfer function (6.10) must have second order zero at $z = 1$, say $r_1 = r_2 = 1$ and the other zeros and all poles must be located outside of the frequency band of interest. With the assumption $0 \le \phi_i, \psi_i \le 2\pi$ it follows from (6.9), (6.11) and (6.12) that,

$$Q = -(-1)^L |Q| \exp\left\{ \frac{j}{2} \left(\sum_{i=3}^{M} \phi_i - \sum_{i=1}^{N} \psi_i \right) \right\}. \tag{6.14}$$

Next, it is required that each non-hybrid part of the hybrid scheme to be stable within its own domain. From (6.8) it follows,

$$\frac{\mathbf{u}_0^H \mathbf{S}_l \mathbf{u}_0}{\mathbf{u}_0^H \mathbf{M} \mathbf{u}_0} + \frac{1}{\delta t^2} \frac{B(z_0)}{A_l(z_0)} = 0 . \tag{6.15}$$

The first term of (6.15) is nonnegative and bounded by the greatest eigenvalue $\lambda_{\max}$ of matrix equation,

$$\mathbf{S}_l \mathbf{u} = \lambda \mathbf{M} \mathbf{u} . \tag{6.16}$$

Therefore, the transfer function $T(z)$ is suitable for stable time-stepping if for any $0 \le \lambda \le \lambda_{\max}$, the equation,

$$T(z) + \lambda \delta t^2 = 0 \tag{6.17}$$

does not hold true for any $|z| > 1$. According to (6.12), $B(z)$ is of higher order than $A(z)$ and all its roots are located on the unit circle. Therefore, as it was done in the previous

chapter, by examining the plot of $-T(e^{j\omega})$ allows us to determine, $\lambda_{\max} = C_{\max}$ (*see Figure 6.3 and example below*) for which all M roots of (6.17) are located on the unit circle. As an example let us consider,

$$T_e(z) = \frac{B(z)}{A_e(z)} = \frac{(1-z^{-1})^2 B_1(z)}{z^{-1} A_1(z)}, \tag{6.18}$$

for explicit time-stepping and,

$$T_i(z) = \frac{B(z)}{A_i(z)} = \frac{(1-z^{-1})^2 B_1(z)}{0.25 \cdot (1+z^{-1})^2 B_1(z)}, \tag{6.19}$$

for implicit time-stepping of the hybrid scheme. The actual order of the implicit transfer function is two and it is equivalent to one used for implicit time-stepping in (6.1) with $\theta = 1/4$. Extra terms are added to make numerators of (6.18) and (6.19) identical. Next, let us assume that,

$$\begin{aligned} B_1(z) &= (1-rz^{-1})(1-r^* z^{-1}), \\ A_1(z) &= Q(1-pz^{-1})(1-p^* z^{-1}). \end{aligned} \tag{6.20}$$

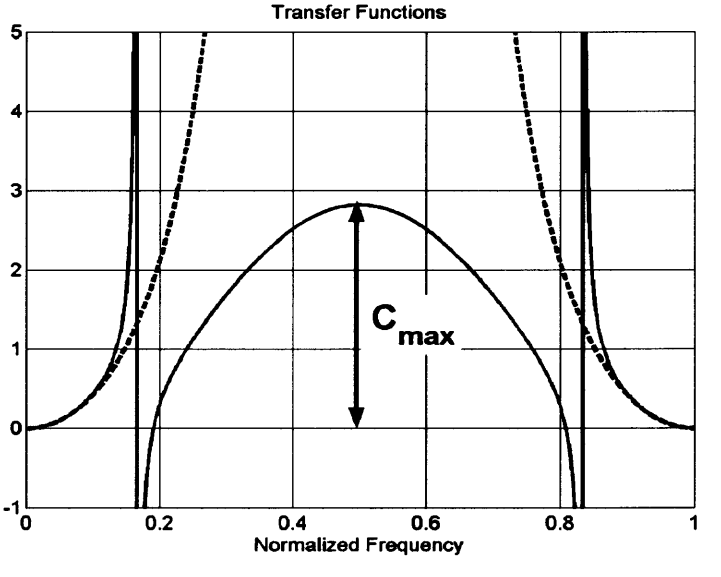

Figure 6.3 Plots of transfer functions(multiplied by -1) for explicit (solid line) and implicit (dashed line) time-stepping.

As it was pointed out in [6] trapezoidal integration with rectangular edge elements makes the mass matrix diagonal and FEM discretization is equivalent to the central difference approximation of spatial derivatives [10]. Therefore, the transfer function (6.18) together with trapezoidal integration will result in fully explicit time-stepping scheme for edges of rectangular elements except for those shared by the unstructured grid.

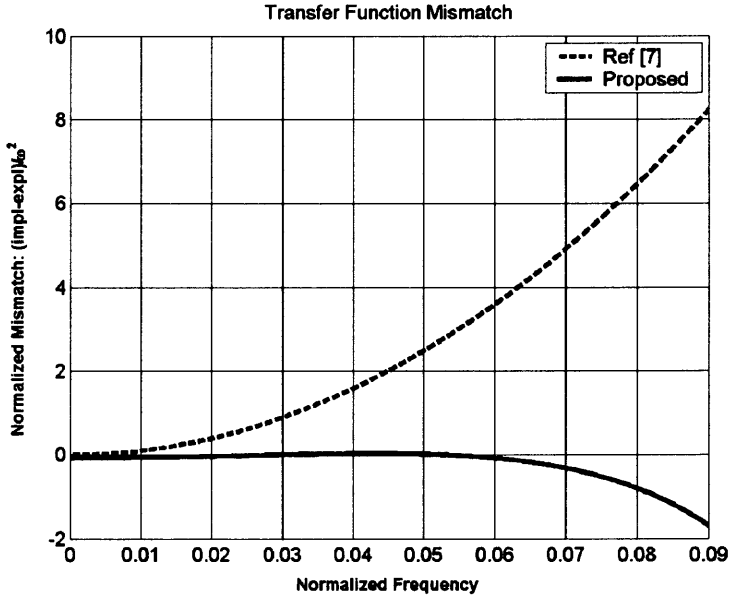

Figure 6.4 Transfer function mismatch.

Since, the roots of polynomials in (6.20) come in complex conjugate pairs, coefficients a_k, b_k in (6.3) and (6.4) are real valued, which is desirable, because complex variables would require more memory storage and also increase math count of the algorithm. Following are parameter values in (6.20) optimized with the help of Matlab function

fmincon [37] to reduce the mismatch between implicit and explicit transfer functions, $\left(T_i\left(e^{j\omega}\right)-T_e\left(e^{j\omega}\right)\right)/\omega^2$, (*see appendix B below*)

$$\begin{aligned} |Q| &= 1.2837, \\ r &= e^{j\phi} = e^{j2\pi\cdot 0.1911}, \\ p &= e^{j\psi} = e^{j2\pi\cdot 0.1661}. \end{aligned} \tag{6.21}$$

It can be seen from the Figure 6.4 that in the numerical frequency range $0.015 < f < 0.06$, $f = \omega/2\pi$ mismatch is virtually eliminated. This frequency range corresponds to three dimensional FDTD stability limit with cell size-to-wavelength ratio, $N_\lambda = 20$. Substituting (6.21) into (6.20) gives us transfer function coefficients used for time-stepping (6.8),

$$\begin{aligned} B(z) &= 1-2.7234z^{-1}+3.4469z^{-2}+2.7234z^{-3}+z^{-4} \\ A_e(z) &= 1.2837z^{-1}-1.2917z^{-2}+1.2837z^{-3} \\ A_i(z) &= 0.25+0.31914z^{-1}+0.13828z^{-2}+0.31914z^{-3}+0.25z^{-4}. \end{aligned} \tag{6.22}$$

Owing to the special choice (6.20), coefficients of polynomials (6.22) are symmetric with respect to the middle one, which means that terms with identical multipliers in (6.3) and (6.4) can be combined to reduce math count of the algorithm. With the use of (6.14) and (6.20), equation (6.8) becomes,

$$1 = F(\omega) \equiv \frac{4}{\delta t^2} \times \frac{\alpha \sin^2\left(\frac{\omega}{2}\right)\sin\left(\frac{\phi-\omega}{2}\right)\sin\left(\frac{\phi+\omega}{2}\right)}{\beta|Q|\sin\left(\frac{\psi-\omega}{2}\right)\sin\left(\frac{\psi+\omega}{2}\right)+\gamma\cos^2\left(\frac{\omega}{2}\right)\sin\left(\frac{\phi-\omega}{2}\right)\sin\left(\frac{\phi+\omega}{2}\right)}. \tag{6.23}$$

where, $\alpha = \mathbf{u}_0^H\mathbf{M}\mathbf{u}_0$, $\beta = \mathbf{u}_0^H\mathbf{S}_e\mathbf{u}_0$ and $\gamma = \mathbf{u}_0^H\mathbf{S}_i\mathbf{u}_0$ are contributions from explicit and implicit elements respectively. Before analyzing (6.23) it should be to pointed out that parameters in (6.21) satisfy,

$$0 < \psi < \phi < \pi. \tag{6.24}$$

Below it is proven that for time-steps slightly less than the stability limit of conventional

FDTD, equation (6.23) has all its three roots located on the unit circle $|z| = |e^{j\omega}| = 1$.

Both additive terms in the denominator of $F(\omega)$ are positive for $0 < \omega < \psi, \phi$ and negative for $\psi, \phi < \omega < \pi$. Therefore, the denominator has a zero between ψ and ϕ, and it does not have any other zeros for $0 < \omega < \pi$. Also there is a complex conjugate zero in the range, $2\pi - \phi < \omega < 2\pi - \psi$. It means that the plot of $F(\omega)$ should look like the solid line on Figure 6.3. Let us estimate the local maximum of $F(\omega)$ in the vicinity, $f = \omega/2\pi \approx 0.5$,

$$C_{\max} \equiv F(\omega_{\max}) \geq F(\pi) = \frac{\alpha}{\delta t^2 \beta} \cdot \frac{4\cos^2\left(\frac{\phi}{2}\right)}{|Q|\cos^2\left(\frac{\psi}{2}\right)} \tag{6.25}$$

Stability limit for conventional FDTD is give by $\Delta t_{CFL}^2 = 2/\sqrt{\lambda_{\max}}$, [7] and therefore, we have,

$$\frac{\alpha}{\beta} \geq \frac{1}{\lambda_{\max}} = \frac{\Delta t_{CFL}^2}{4}. \tag{6.26}$$

From (6.25) and (6.25) it follows that,

$$F(\omega_{\max}) \geq \left(\frac{\Delta t_{CFL}}{\delta t}\right)^2 \cdot \frac{\cos^2\left(\frac{\phi}{2}\right)}{|Q|\cos^2\left(\frac{\psi}{2}\right)} = \left(\frac{0.84\Delta t_{CFL}}{\delta t}\right)^2. \tag{6.27}$$

According to (6.20), polynomials, $B(z), A_e(z), A_i(z)$ involved in (6.8) are of forth order, therefore, equation (6.23) can have only four solutions. From (6.25), (6.27) and by observing Figure 6.3, it follows that all four solutions of (6.23) are located on the unit circle $0 \leq \omega \leq 2\pi$ if time-step in (6.2) is 16% below the stability limit of conventional FDTD. This in turn means that, hybrid time-marching according to (6.2) does not have solutions exponentially growing with number of time-steps, i.e. it is stable.

6.4 Numerical Example

Modulated Gaussian source $\sin(\Omega t)e^{-(t/t_0)^2}$ was injected from the left side. Propagating pulse was reflected from the grid interface and is show in Figure 6.5 for hybrid of [7] and in Figure 6.6 for the proposed hybrid scheme. If grid spacing in (3.8) is chosen $1/20^{th}$ of the wavelength, then the stability limit of three-dimensional FDTD is $\delta t = \lambda/(20\sqrt{3}c)$ which about $1/35^{th}$ of the wave period. Therefore, period of the Gaussian pulse was set equal to 30 time-steps, which means that, at the corresponding numerical frequency $f = 1/30 = 0.033$ the transfer function mismatch is virtually nonexistent, as it can bee seen from Figure 6.4. Pulse duration t_0 was equal to two periods or sixty time-steps. Cells up to cell number 3000 were time-stepped explicitly, from cell number 3000 implicit finite-element time-domain method with trapezoidal integration was used to update field values. Trapezoidal integration of stiffness and mass matrices makes FEM and FDTD spatial discretization equivalent, so that the reflection from the interface between different types of the grid was only due to the transfer function mismatch. From Figures 6.5 and 6.6 it can be seen that as a result of minimum mismatch around the central frequency of the pulse, $f = 0.033$, the reflected wave amplitude was reduced by about two orders of magnitude.

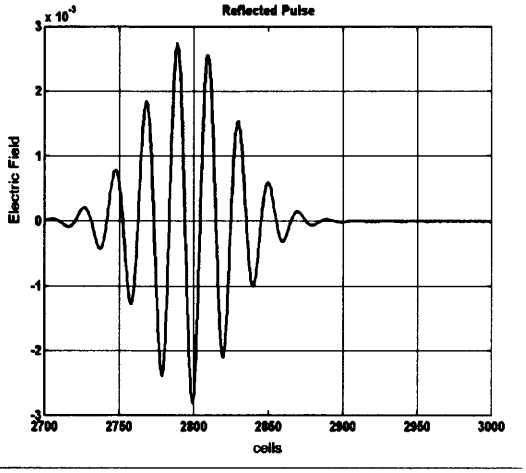

Figure 6.5 Reflection from grid interface for hybrid of Rylander and Bondeson [7]

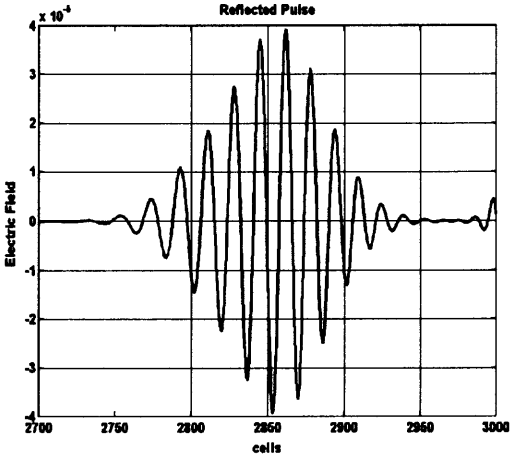

Figure 6.6 Reflection from grid interface for the proposed hybrid algorithm.

6.5 Discussion

Implementation of hybrid time-marching (6.2) according to the choice (6.22) requires storage of four previous field values, whereas hybrid of [7] requires storage of two previous field values. Operational count of the proposed algorithm is increased by at most four multiplications and four additions per time-step for every edge, which should be negligible in three dimensional simulations, especially when higher order elemental functions are used [4].

Stability limit of the proposed hybrid time-stepping, defined by (6.22), was reduced by 16% compared to conventional FDTD. Tuning reflection error and stability limit for a specific frequency band can be done easily with the help of Matlab optimization toolbox [37] or, any other software package capable of nonlinear optimization.

Nonphysical reflection can play important role in modeling structures with very week physical reflection. Typical example could be low-pass microwave filter simulation; low-pass filters are designed to have very small reflection coefficient. Although, nonphysical reflection may be small compared to the incident pulse, it can alter physical reflected pulse and introduce high error to the reflection coefficient estimation. Another example is the design of optical resonators in which any local artificial reflection may be amplified and resulted in severe errors.

CHAPTER 7

CONCLUSION

7.1 Discussion of Results

In this investigation, stability and time-discretization error of FDTD was analyzed using Z-Transform technique. Central-difference approximation of time derivative was generalized as a discrete-time linear time-invariant system with rational transfer function. Empirical procedure to optimize transfer function is presented. It was shown that by manipulating coefficients of transfer function it is possible to significantly reduce time-sampling error in the desired frequency range. Examples of optimized transfer functions were presented. The resulting time-stepping was fully explicit and had lower time-sampling compared to the central difference approximation of original FDTD. Stability limit of the original formulation was preserved.

Possibility of implicit scheme is also considered. Implicit time-stepping is unconditionally stable and requires matrix inversion at every time-step. Matrix inversion is computationally very intensive. Therefore, it desirable to keep time-step size of explicit algorithm as large as possible. Within the framework of the developed theory a novel implicit time-stepping scheme is presented. New implicit scheme has low sampling error for values of numerical frequency close to theoretical limit dictated by Nyquist's sampling theorem.

Improved Explicit-Implicit Hybrid FDTD-FEM solver for Maxwell's time-dependant equations was developed. Hybrid algorithm employs computationally efficient FDTD to solve large homogeneous volumes, and FEM with boundary conforming

unstructured grid around curved boundaries. If computationally extensive FEM is limited to small volumes around curved boundaries, then the computational efficiency of original FDTD is preserved.

The main issue of any hybrid solver, nonphysical reflection from the interface between FDTD and FEM sections of the grid, was addressed. Proposed hybrid algorithm replaces conventional central-difference approximation of second order time-derivative with a rational transfer function discrete-time linear time-invariant system. Stability of the formulation was rigorously proven for the general three dimensional case. Coefficients of time-discretization can be optimized for the best performance in the desired band of frequencies. Procedure to optimize transfer function and at the same time to preserve stability of algorithm is derived. Example of transfer functions with low reflection error is discussed. Numerical examples demonstrated the stability the proposed algorithm. Nonphysical reflected wave amplitude was reduced by two orders of magnitude compared to the original hybrid formulation.

7.2 Final Words

FDTD and FEM are major numerical techniques to solve Maxwell's equations for electromagnetics. FDTD employs explicit time-stepping on structured grid with rectangular cells. Therefore it is easy to implement and suitable for parallel processing. Time-marching of FDTD conditionally stable: time-step size is subject to Courant stability limit. In many cases FDTD numerical solution yields good results if grid with cell is chosen about $1/20^{th}$ of the source wavelength. FDTD structure grid results in

staircase approximation of curved boundaries. This together with time-step bound is on the most limiting factors of FDTD.

FEM is often used for numerical solution electromagnetic problems in frequency domain. FEM is formulated on unstructured nonuniform grid. Unstructured grid is well suited for approximation of curved boundaries. Accuracy of FEM depends on grid quality. High quality grid generation is difficult task and can greatly increase computational complexity of the technique.

FDTD and FEM are complementary techniques. FDTD is efficient if staircase approximation can be avoided. FEM is best to use when boundary conforming grid is needed. It is possible to combine FDTD and FEM into hybrid solver. A hybrid solver uses FDTD in larger homogeneous volumes, and FEM near complex boundaries. Limiting computationally intensive FEM to small volumes around curved boundaries allows to maintain computational efficiency of the original FDTD. This way, a hybrid solver can take advantages of FDTD and FEM, and at the same time avoid disadvantages inherent to both of them.

The main disadvantage of a hybrid-solver is the nonphysical reflection from the interface between different types of the grid. Reflection error can be controlled by optimizing time-stepping coefficients.

APPENDIX A

COMMENT ON THE DESIGN OF TRANSFER FUNCTIONS

Stability condition (5.22) MAY be interpreted as a polynomial roots localization problem: time-stepping scheme is stable if all roots of the following polynomial equation,

$$B_H(z)B_E(z)+CA_H(z)A_E(z)=0, \tag{A.1}$$

are located within the unit circle $|z|\le 1$ for all possible values of parameters C. Procedure described in Chapter 5 allows to localize all roots of equation (A.1) on the unit circle. This is done by posing restrictions on the roots of numerator and denominator of the transfer function. Another approach would be to start without any restriction and check if all roots of (A.1) are located within the unit circle for all $0 \le C \le C_{\max}$. To do so, equation (A.1) need not be solved explicitly. Any stability test, such as Shür-Cohn criteria [8] allows to test allows to check if all roots of a given polynomial are located within the unit circle without actually solving for them. Steps to design such transfer function are as follows [24]:

1. Start with an initial guess for transfer function coefficients with low sampling error.
2. Use a test such as Shür-Cohn criteria, to determine the range $0 \le C \le C_{\max}$ for which all roots of equation (A.1) are located within the unit circle.
3. Stability limit for the transfer function is given by,

$$\delta t_{\max} = \Delta t_{CFL} \frac{C_{\max}^{1/2}}{2}. \tag{A.2}$$

Advantage of the above procedure is that, it does not pose any restrictions on polynomials roots. Therefore, it may result in a more optimal solution compared to the one described in Chapter 5. However, such tests, e.g. Shür-Cohn criteria, are *aposteriori* test, once the transfer function has been identified (*see reference* [36] *and Chapter 5 of this dissertation*).

APPENDIX B

HYBRID TRANSFER FUNCTION OPTIMIZATION

B.1 Mathematical Procedure

The objective of the optimization process is to reduce mismatch between explicit and implicit transfer functions on both sizes on the interface. These transfer functions are defined in (6.18) and (6.19), respectively, in the frequency range, $0.015 < f < 0.06$. The implicit transfer function is not affected by the optimization process. Its values on the unit circle are given by,

$$T_i\left(e^{j\omega}\right) = -4\tan^2\left(\frac{\omega}{2}\right). \tag{B.1}$$

Substituting (6.20) into (6.18) and recalling that $r = e^{j\phi}$, $p = e^{j\psi}$, results in,

$$T_e\left(e^{j\omega}\right) = -\frac{4\sin^2\left(\frac{\omega}{2}\right)\sin\left(\frac{\omega-\phi}{2}\right)\sin\left(\frac{\omega+\phi}{2}\right)}{Q\sin\left(\frac{\omega-\psi}{2}\right)\sin\left(\frac{\omega+\psi}{2}\right)}. \tag{B.2}$$

The normalized mismatch parameter is defined as,

$$\delta T\left(e^{j\omega}\right) = \frac{\left|T_i\left(e^{j\omega}\right) - T_e\left(e^{j\omega}\right)\right|^2}{\omega^2}. \tag{B.3}$$

Equation (B.3) defines a mismatch for single frequency. Mismatch for a range of frequencies is defined simply by an integration:

$$\Delta T = \int_{\omega_{\min}}^{\omega_{\max}} \delta T\left(e^{j\omega}\right) d\omega. \tag{B.4}$$

The mismatch (B.4) depends on three real valued parameters Q, ϕ, ψ and can be minimized with fmincon *function* from Matlab optimization toolbox [37]. The choice

$$Q = 1,\ \phi = 0,\ \psi = 0, \tag{B.5}$$

is equivalent to the time stepping procedure in a conventional FDTD and therefore, can be used as a starting point. During the optimization process, parameter Q should be kept positive. Zeros and poles of transfer of function should be kept outside of the frequency range of interest and satisfy the relation,

$$\omega_{\max} + \delta\omega < \psi \le \phi \le \pi, \tag{B.6}$$

where, $\delta\omega$, is small and positive. The integral in (B.4) can be evaluated using trapezoidal integration rule.

B.2 The Optimization Process

1. Create a function ΔT, which accepts Q, ϕ, ψ as arguments and computes mismatch (B.4) using trapezoidal integration rule. Number of nodes for trapezoidal integration can be small, namely in the range of 20 to 100
2. Use $Q = 1,\ \phi = 0,\ \psi = 0$ as the starting guess.
3. During the optimization process, variables must be subject to the bound $1.1 \cdot \omega_{\max} + < \psi \le \phi \le \pi$, $0.1 < Q < 10$
4. Stability bound, $C_{\max}$, can be controlled by forcing $|\phi - \psi| < \zeta$. Smaller ζ, results in a higher stability limit; larger ζ results in a lower mismatch

APPENDIX C

HYBRID TIME-STEPPING IMPLEMENTATION

Once a spatial grid is generated, stiffness and mass matrices can be assembled from the elemental matrices (2.40) by using conversion from local to global indices [4]. Time-stepping of the electric field is performed according to the following procedure:

1. Edges of a structured grid, not shared by unstructured grid, are updated explicitly using the central difference approximation of spatial derivatives,

$$-\frac{b_0}{\delta t^2}\mathbf{M}\mathbf{u}^n = \frac{1}{\delta t^2}\mathbf{M}\sum_{k=1}^{M} b_k \mathbf{u}^{n-k} + \mathbf{S}_e \sum_{k=1}^{N} a_k^{(e)} \mathbf{u}^{n-k} + \mathbf{f}^n \qquad \text{(C.1)}$$

2. Edges of unstructured grid are updated implicitly. Contribution to the right hand side from explicitly updated edges are computed using global indices of shared edges; edges belonging to interface elements of the structured grid are computed according to

$$-\left(\frac{b_0}{\delta t^2}\mathbf{M} + a_0 \mathbf{S}_i\right)\mathbf{u}^n = \frac{1}{\delta t^2}\mathbf{M}\sum_{k=1}^{M} b_k \mathbf{u}^{n-k} + \mathbf{S}_i \sum_{k=1}^{N} a_k^{(i)} \mathbf{u}^{n-k} + \left[\mathbf{S}_e \sum_{k=1}^{N} a_k^{(e)} \mathbf{u}^{n-k}\right]_i + \mathbf{f}^n. \qquad \text{(C.2)}$$

REFERENCES

[1] K. S. Yee, *"Numerical Solution of Initial Boundary Value Problems Involving Maxwell's Equations in Isotropic Media,"* IEEE Trans. Antennas Propagat., Vol. 14, 1966, pp. 302-307.

[2] Allen Taflove, Susan Hagness, *"Computational Electrodynamics: The Finite-Difference Time-Domain Method,"* 2 ed., Artech House, Boston, MA, 2000.

[3] Kurt. L. Shlager, John. B. Schneider, *"A Survey of the Finite-Difference Time-Domain Literature,"* in Advances in Computational Electrodynamics: The Finiye-Difference Time-Domain Method, A. Taflove, Ed. Norwood, MA: Artech House, 1998, ch. 1.

[4] Jianming Jin, *"The Finite Element Method in Electromagnetics,"* 2nd ed., John Wiley & Sons, 2002.

[5] F. Zheng, Z. Chen, J. Zhang, *"Toward the Development of a Three-Dimensional Unconditionally Stable Finite-Difference Time-Domain Method,"* IEEE Trans. Microwave Theory Tech., Vol. 48, Sept. 2000, pp. 1550-1558.

[6] T. Rylander, A. Bondeson, *"Stable FEM-FDTD hybrid method for Maxwell's equations,"* Comp. Phys. Com. 125 (2000) 75–82.

[7] T. Rylander, A. Bondeson, *"Stability of Explicit-Implicit Hybrid Time-Stepping Schemes for Maxwell's Equations,"* Journal of Computational Physics 179, 426–438 (2002).

[8] John G. Proakis, Dimitris G. Manolakis, *"Digital Signal Processing: Principles, Algorithms and Applications" 3rd ed.*, Prentice Hall, 1995.

[9] Alan V. Oppenheim, Ronald W. Schafer, and John R. Buck, *"Discrete-Signal Processing," 2nd ed.*, Prentice Hall, 1999.

[10] Paul H. Aoyagi, Jin-Fa Lee, Raj Mittra, *"A Hybrid Yee Algorithm/Scalar Wave Equation Approach,"* IEEE Tran. Antennas Propagat. Vol. 41, September 1993.

[11] H. Whitney, *"Geometric integration theory,"* Princeton University Press, 1957.

[12] J. C. Nedelec, *"Mixed Finite Elements in R^3,"* *Numer. meth.*, Vol. 35, pp. 315-341.

[13] M. Ghrist, B. Fornberg, T. B. Driscoll, *"Staggered Time Integration for Wave Equations,"* SIAM J. Numer. Anal., Vol. 38, No, 3, pp 718-741.

[14] Patric M. Knupp, Stanly Steinberg, *"Fundamentals of Grid Generation"*, CRC Press, Jan. 1994.

[15] A. C. Cangellaris, D. B. Wright, *"Analysis of the numerical error caused by the stair-stepped approximation of a conducting boundary in FDTD simulations of electromagnetic phenomena,"* IEEE Trans. Antennas Propagat., Vol. 39, Oct. 1991.

[16] Gedney, S., F. Lansing and D. Rascoe, *"Full wave analysis of microwave monolithic circuit devices using a generalized Yee-algorithm based on an unstructured grid,"* IEEE Trans. Microwave Theory and Techniques, Vol. 44, 1996, pp. 1393-1400.

[17] S. Gedney, F. Lansing, R. T. Kihm, N. Owona, K. Virga, *"Simulating "large" microwave circuits with the parallel Planar Generalized Yee algorithm,"* IEEE Symp. Digest, IEEE MTT-S International, Vol 2, 17-21, June 1996, pp. 1011-1014.

[18] S. Gedney, F. Lansing, *"Nonorthogonal and Unstructured Grids,"* Chapter 11 in reference [2].

[19] A. Taflove, M. E. Brodwin, *"Numerical solution of steady-state electromagnetic problems using the time-dependant Maxwell's equations,"* IEEE Trans. Microwave Theory Tech., Vol. 23, 1975, pp. 623.

[20] J. W. Thomas, *"Numerical Partial Differential Equations: Finite Difference Methods,"* Springer-Verlag, 1999.

[21] A. I. Markushevich, *"Theory of Functions of a Complex Variable,"* Chelsea Pub Co; 2nd edition (June 1, 1985).

[22] B. P. Lathi, *"Signal Processing and Linear Systems,"* Oxford University Press, 1998

[23] D. M. Sullivan, *"Z-Transform theory and FDTD method,"* IEEE Trans. Antennas Propagat., Vol. 44, Jan. 1996 pp. 28 -34.

[24] W.H. Weedon, C. M. Rappaport, *"A general method for FDTD modeling of wave propagation in arbitrary frequency-dispersive media,"* Antennas and Propagat., IEEE Transactions on , Vol. 45, March 1997, pp. 401 -410.

[25] Kurt L. Shlager, John B. Schneider, *"Comparison of the Dispersion Properties of Several Low-Dispersion Finite-Difference Time-Domain Algorithms,"* IEEE Trans. Antennas Propagat., Vol. 51, Mar. 2003, pp. 642-653.

[26] D. J. Riley, C. D. Turner, *"Interfacing Unstructured Tetrahedron Grids to Structured-Grid FDTD,"* IEEE Microwave and Guided Wave Letters, Vol. 5, No. 9, Sept. 1995, pp. 284-286.

[27] R-B Wu, T. Itoh, *"Hybrid Finite-Difference Time-Domain Modeling of Curved Surfaces Using Tetrahedral Edge Elements,"* IEEE Trans. Antennas Propagat., Vol. 45, No. 8, August 1997, pp. 1302-1309.

[28] A. Monorchio, R. Mittra, *"A Hybrid Finite-Element Finite-Difference Time-Domain (FE/FDTD) Technique for Solving Complex Electromagnetic Problems,"* IEEE Microwave and Guided Wave Letters, Vol. 8, No. 2, Feb. 1998, pp. 93-95.

[29] A. Monorchio, A.R. Bretones, R. Mittra, G. Manara, R. G. Martin, *"A hybrid time-domain technique that combines the finite element, finite difference and method of moment techniques to solve complex electromagnetic problems,"* IEEE Trans. Antennas Propagat., Vol. 52 , Oct. 2004, pp. 2666-2674.

[30] Yee, K. S.; Chen, J. S.; Chang, A.H., *"Numerical experiments on PEC boundary condition and late time growth involving the FDTD/FDTD and FDTD/FVTD hybrid,"* Antennas and Propagation Society International Symposium, 1995. AP-S. Digest, Volume: 1 , 18-23 June 1995, pp. 624 - 627 Vol. 1.

[31] C-T Hwang, R-B Wu, *"Treating late-time instability of hybrid finite-element/finite-difference time-domain method,"* IEEE Trans. Antennas Propagat., Vol. 47, Feb 1999, pp. 227-232.

[32] M. Marrone, R. Mittra, *"A Theoretical Study of the Stability Criteria for Hybridized FDTD Algorithms for Multiscale Analysis,"* IEEE Trans. Antennas Propagat, Vol. 52 Aug. 2004, pp. 2158-2167.

[33] A. Monorchio, E. Martini, G. Manara, G. Pelosi, *"A Dispersion Analysis for the Finite-Element Method in Time Domain With Triangular Edge Elements,"* IEEE Trans. Antennas Propagat. Letters, Vol 1, 2002, pp. 207-210.

[34] Jin-Fa Lee, Robert Lee, Andreas Cangellaris, *"Time-domain Finite-Element Methods,"* IEEE Trans. Antennas Propagat., Vol. 45, No.3, March 1997, pp. 430-444.

[35] Coulomb, J.-L.; Zgainski, F.-X.; Marechal, Y., *"A pyramidal element to link hexahedral, prismatic and tetrahedral edge finite elements,"* IEEE Trans. Magnetics, Vol. 33, March 1997, pp. 1362-1365.

[36] K. Abdijalilov, H. Grebel, *"Z-transform Theory and FDTD Stability,"* IEEE Trans. Antennas Propagat., Vol. 52, Nov. 2004, pp. 2950 - 2954.

[37] MathWorks Matlab Optimization Toolbox v.2.2(R13).